UNIVERSITY OF ALBERTA

Parameterization of Ice Crystal Aggregation

By

Christine C. Nam

©

A thesis submitted to the Faculty of Graduate Studies and Research in partial fulfillment of the requirements for the degree of Master of Science

Department of Earth and Atmospheric Sciences

Edmonton, AB

Spring 2005

0-494-08124-4

Library and Archives Canada

Published Heritage Branch

395 Wellington Street
Ottawa ON K1A 0N4
Canada

Bibliothèque et Archives Canada

Direction du Patrimoine de l'édition

395, rue Wellington
Ottawa ON K1A 0N4
Canada

Your file *Votre référence*
ISBN:
Our file *Notre reference*
ISBN:

NOTICE:
The author has granted a non-exclusive license allowing Library and Archives Canada to reproduce, publish, archive, preserve, conserve, communicate to the public by telecommunication or on the Internet, loan, distribute and sell theses worldwide, for commercial or non-commercial purposes, in microform, paper, electronic and/or any other formats.

The author retains copyright ownership and moral rights in this thesis. Neither the thesis nor substantial extracts from it may be printed or otherwise reproduced without the author's permission.

AVIS:
L'auteur a accordé une licence non exclusive permettant à la Bibliothèque et Archives Canada de reproduire, publier, archiver, sauvegarder, conserver, transmettre au public par télécommunication ou par l'Internet, prêter, distribuer et vendre des thèses partout dans le monde, à des fins commerciales ou autres, sur support microforme, papier, électronique et/ou autres formats.

L'auteur conserve la propriété du droit d'auteur et des droits moraux qui protège cette thèse. Ni la thèse ni des extraits substantiels de celle-ci ne doivent être imprimés ou autrement reproduits sans son autorisation.

In compliance with the Canadian Privacy Act some supporting forms may have been removed from this thesis.

While these forms may be included in the document page count, their removal does not represent any loss of content from the thesis.

Conformément à la loi canadienne sur la protection de la vie privée, quelques formulaires secondaires ont été enlevés de cette thèse.

Bien que ces formulaires aient inclus dans la pagination, il n'y aura aucun contenu manquant.

Canada

ABSTRACT

This thesis develops an ice aggregation parameterization scheme for Numerical Weather Prediction models. It incorporates ice crystal terminal fall velocities and cross-sectional areas which depend on air temperature.

The aims of this thesis are (i) to determine the effects of temperature on the aggregation rate of cloud ice crystals by snow aggregates, and (ii) to quantify the effects of snow aggregate size distributions of the same mass, but varying in broadness, on the collection rate. The results show that for subfreezing conditions the ice aggregation rate increases with increasing temperature. The effects of size distribution on collection rate can be shown by assuming snow aggregate size distributions are of the same mass but varying in broadness. The results indicate size distributions consisting of a greater number of larger particles result in a faster aggregation rate.

TABLE OF CONTENTS

			Page
1		INTRODUCTION	1
	1.1	Aggregation of ice crystals to form snow	1
	1.2	Numerical models of snow storms	3
	1.3	Parameterization of aggregation	4
	1.4	Statement of research objectives	5
	1.5	Organization of thesis	6
2		MICROPHYSICAL EQUATIONS FOR ICE AGGREGATION	7
	2.1	Shapes of ice crystals	7
	2.2	Mass of ice crystals and snow aggregates	8
	2.3	Terminal fall velocities of ice crystals and snow aggregates	9
	2.4	Mass growth of a snow aggregate by collection of ice crystals	11
	2.5	Expected differential velocity	12
	2.6	Collection efficiency	14
	2.7	Summary	17
3		PARAMETERIZATION OF ICE AGGREGATION	19
	3.1	Snow aggregate size distribution	19
	3.1	Previous aggregation parameterizations	21
	3.2	Control case	23
4		EFFECTS OF TEMPERATURE ON RATE OF AGGREGATION	25
	4.1	Verification of parameterization scheme for rate of ice aggregation	25
	4.2	Geometric collection rate	27
	4.3	Comparison of collection rates	28
	4.4	Combining the collection rate by aggregation and mass growth rate by diffusion	29
	4.5	Summary	31

5		EFFECTS OF SNOW AGGREGATE SIZE DISTRIBUTION ON COLLECTION RATE	32
	5.1	Effects of snow aggregate size distributions on the collection rate	32
	5.2	Duration of snow formation	33
	5.3	Summary	35
6		GROWTH BY ICE AGGREGATION VERSUS DEPOSITION-DIFFUSION	36
	6.1	Fractional rate of increase of mass due to ice aggregation	36
	6.2	A comparison of the fractional rate of increase of mass by aggregation to the fractional rate of increase of mass by diffusion	37
	6.3	Summary	38
7		CONCLUSIONS AND FUTURE WORK	39
	7.1	Conclusions	39
	7.2	Future work	41
		FIGURES	44
		REFERENCES	57
		APPENDIX A: List of symbols	60
		APPENDIX B: Fall velocity	61
		APPENDIX C: Collection rate (Rate of aggregation)	63
		APPENDIX D: Doubling time	64
		APPENDIX E: Maximum fall times and distances	66

LIST OF TABLES

Table		Page
2.1	Fall velocity parameters as a function of air temperature.	10
4.1	The hypothesized snow aggregate size and composition, according to temperature (°C), based on the diffusional and aggregate growth.	30
5.1	Aggregation rates as a function of characteristic diameter (D_m) for selected temperatures. The values are expresses as a ratio of $C(D_m)/C(D_{m0}) = C/C_o$.	33
5.2	Doubling times (τ) as a function of characteristic diameter (D_m) for selected temperatures.	35
6.1	Growth by aggregation vs. diffusion for plates and dendrites weighing 10^{-8} to 10^{-6}g.	38

LIST OF FIGURES

Figure		Page
1.1	A schematic representation of typical ice crystal shapes.	44
1.2	An ice crystal classification scheme as a function of temperature (°C) and excess vapour density over ice saturation (g m^{-3}) adopted from Kobayashi's (1958).	45
2.1	The fall velocity (cm s^{-1}) of plate and dendrites snow aggregates as a function of unmelted diameter (cm).	46
2.2	A comparison of the collection efficiencies (E) of Lin *et al.* (1983), Cotton *et al.* (1986), and Khain and Sednev (1996).	47
3.1	A typical inverse exponential snow aggregate size distribution $N(D_a)$.	48
4.1	The geometric collection rates (g g^{-1} s^{-1}) of the control case, Lin *et al.* (1983), and Cotton *et al.* (1986) versus temperature (°C).	49
4.2	The collection rates (g g^{-1} s^{-1}) of the control case, Lin *et al.* (1983), and Cotton *et al.* (1986) versus temperature (°C). The collection rate of Khain and Sednev (1995) at -12°C, is denoted by +	50
5.1	The snow aggregate size distributions (cm^{-4}) with characteristic diameters equal 50, 75, 100, 150, 200, and 250% of the control case characteristic diameter (D_{mo} = 0.33 cm).	51

5.2 The collection rates (g g^{-1} s^{-1}) with snow aggregates size distributions with characteristic diameters equal 50, 75, 100, 150, 200, and 250% of the control case characteristic diameter (D_{mo} = 0.33 cm). 52

5.3 The time (min) required for the mixing ratio of snow aggregates to double for collection rates with size distributions using characteristic diameters equal 50, 75, 100, 150, 200, and 250% of the control case characteristic diameter (D_{mo} = 0.33 cm). 53

6.1 The fractional rate of increase of mass (s^{-1}) by aggregation of plates at -5°C, sector plates at -10°C, and dendrites at -15°C. 54

6.2 The fractional rate of increase of mass (s^{-1}) by aggregation and diffusion of plates at -5°C and dendrites at -15°C. 55

7.1 The maximum time (min) and maximum distance (km) required for a snow aggregate's diameter to grow from 0.005 to 0.15 cm versus temperature (°C). 56

1. INTRODUCTION

Aggregation of ice crystals to form snow

A common form of precipitation in mid-latitude winters is snow. Approximately half of the annual precipitation of Alberta occurs in the form of snow (~150 cm, Reuter and Beaubien, 1996). In fact, most of the precipitation which falls as rain at the surface originates from melting snow formed at higher, colder altitudes. The central task of precipitation physics is thus to explain how snowflakes can be created by aggregation of ice crystals in times as short as 30 minutes. This is approximately the time interval observed between the initial development of a convective cloud and the first appearance of surface snowfall or melted rainfall. During this 30 min interval, a snowflake must be formed by the aggregation of numerous individual ice crystals. Cloudy air consists of ice crystal concentrations of approximately 50 ice crystals per liter, averaging about 25 μm in size, which evolves into a snowflake population of about 0.05 snowflakes per liter with typical sizes of 250 μm (Rogers and Yau, 1989, p.150 & 164). This 10-fold increase in size is accounted for mostly by collision and adhesion of individual ice crystals.

In principle, the aggregation process can be modeled by the classical Stochastic Collection Equation that simulates the interaction of individual particles by prescribing a collection kernel (see Khain and Sednev, 1995). The formulation of the collection kernel, however, is complicated by the intricate geometries and orientations of the falling pristine crystals. In addition, the fact that ice crystals do not always coalesce once they have made physical contact also adds to the complexity. The probability of adhesion depends on air temperature and ice crystal shape, with delicately branched dendrites having a higher probability of adhesion than columns. Adhesion is greatest near 0°C and decreases with decreasing temperature. The largest snow aggregate sizes were observed near 0°C by Hobbs *et al.* (1974) with size decreasing with decreasing temperature with the exception of a secondary maximum size between -10 and -15°C. Hobbs *et al.* (1974) believe the secondary maximum is the result of the intricate

structure of dendritic crystals being more conducive to the formation of snow aggregates.

The size and shape of snow aggregates are irregular due to the complexity in ice crystal shape and the various settling and adhesion orientations of the ice crystals forming the snow aggregate. Ice crystal shapes can be classified into three main groups; columns, plates, and dendrites (Figure 1.1, Rogers and Yau, 1989, p.162). An individual ice crystal's shape is dependent on the ambient temperature and excess vapour density over ice saturation (Figure 1.2, Rogers and Yau, 1989, p.163). The spatial size of an individual ice crystal is usually described by the length of its longest axis.

Another complicated aspect of snow aggregation theory is that ice crystals and snow aggregates exhibit fluctuations in their terminal fall velocities. These fluctuations are caused by the shape and orientation of falling ice crystals which affects the aerodynamic drag forces. Thus, in addition to the differential responses to the earth's gravitational field, there are differential responses to the air turbulence in atmospheric motion. The impact of fluctuations on ice crystals' velocities is that crystals of equal size can collide and coalesce.

It is clear from these introductory comments that aggregation involves complicated processes, about which a great deal still needs to be learned. On the other hand, there is an acute need to model numerically the aggregation process to allow for accurate and time efficient computations that predict the snowfall in numerical weather prediction models. Reliable forecasting of precipitation is considered to be advantageous to users of weather forecasting information; in recent years there is an additional requirement not only to forecast the occurrence of snow, but also the amount accumulated. Dupilka and Reuter (2004) showed that Quantitative Precipitation Forecasts (QPF) obtained by operational numerical weather prediction models still lack reliability, particularly for heavy snowfall events.

This thesis focuses on modeling the ice aggregation process to be used within a numerical weather prediction model. This means the aggregation modeling scheme has to be economical in terms of computational resources (i.e. computer memory space and computing time). To introduce our modeling scheme, we have to provide some essential background on numerical models of snowstorms.

1.2 Numerical models of snowstorms

The physical processes operating within a snowstorm are complex and nonlinear. Laboratory experiments and analytical techniques do not lend much insight into the nature of storms. For this reason, research into the dynamics and physics of snowstorms employ numerical simulations as a tool in understanding the behavior of storms. As computers become increasingly powerful, and computational techniques more refined, an increased use of this technique is expected. The immediate goal of numerical simulation is to produce an analog of a phenomenon, faithful to the phenomenon itself, such that the physics can be explored using the model output as a proxy for real observations. A great strength of models is that if they are successful in replicating observations, they can be used to test predictions about nature, and drive toward a true understanding by doing comparative experiments in which initial or boundary conditions are altered. Furthermore, numerical modeling can be used for predictions of future weather if initialized with current observational data.

Numerical models of atmospheric motion consist of approximations to a set of coupled nonlinear partial differential equations. These equations arise from imposing conservation of momentum, energy, and water substances. In numerical cloud or mesoscale models both the space and the time derivatives of the partial differential equations are expressed as finite differences so that the equations become difference equations. The resulting finite difference equations have finite resolution in space and time. The number of computations as well as the storage of variables increases as (Δx Δy Δz) decreases for a specified computational domain size, where Δx, Δy, Δz are the spacing between grid points in the three spatial directions. Moreover, the magnitude of the time step, Δt, is usually restricted by those of Δx, Δy, and Δz, by requirements for the stability of the time integration. Thus an increase of the spatial resolution of a model increases the storage requirements by $(1/\Delta L)^{-3}$, where ΔL is a measure of the spatial resolution, while the number of the computations in a given time interval increases by $(1/\Delta L)^{-4}$.

1.3 Parameterization of aggregation

The processes responsible for forming ice crystals, depositional growth, coagulation of ice crystals, the fall of snowflakes, and sublimation involve complex physics operating on scales far too small to be modeled explicitly. To allow cloud model simulations to be made in feasible times, these microphysical processes must be represented in terms of variables that are explicitly integrated in the numerical model. More specifically, these variables are: ambient temperature (T), density (ρ), mixing ratio of both ice crystals (r_i) and snow aggregates (r_a), and relative humidity (RH).

Ice growing in purely dry growth conditions, that is neglecting any liquid water growth phases, can be described as the compilation of four processes: nucleation of ice crystals, vapor deposition growth of ice crystals, initiation of ice crystal aggregates by collision among ice crystals, and further aggregation by collision among aggregates and ice crystals (Cotton and Anthes, 1989, p.100). The focus of this thesis is on the latter two aggregation processes.

In order to represent aggregation in terms of (T, ρ, r_i, r_a), all low density ice particles in a cloud must be taken into consideration. To do this, a particle size distribution ($N(D_a)$) is assumed. The snow aggregate size distribution is typically represented in one of two ways. The first method, called the Stochastic Collection Equation, assumes the size distribution spectra of snow aggregates $N(D_a)$ is discretized such that $N(D_a)dD_a$ represents the average number of snow aggregates per volume of air whose diameters are between D_a and D_a+dD_a. The evolution of the size spectrum is modeled by predicting the changes in the number of snow aggregates, in the size interval dD_a at a given instant and point in space, through the integration of two differential equations. This method requires large amounts of computing time and storage.

The second method of representing the snow aggregate distribution is called the bulk method. A bulk microphysical parameterization models the evolution of the size spectrum by predicting the changes to the parameters of the analytic function that quantifies the ice crystal size distribution. Because the parameterization scheme does not require a discretization of the size distribution of ice crystals, the storage requirements

and computing time required for microphysical computations are lessened (nearly 100-fold), making it the most effective method of representing aggregation in atmospheric models. Two prominent groups whom we emulate here are Orville's group at the South Dakota School of Mines and Technology (for example, Lin *et al.*, 1983) and Cotton's group at Colorado State University (for example, Cotton *et al.*, 1986). Both Lin *et al.* (1983) and Cotton *et al.* (1986) use an inverse exponential function to represent the snow aggregate size distribution. Lin *et al.* (1983) followed Gunn and Marshall's (1958) snow aggregate size distribution that is based on the droplet diameters created by melted snow. Cotton *et al.* (1986) assumed the *unmelted* snow aggregate size distribution of Rogers (1974). The broadness of Cotton *et al.*'s (1986) snow aggregate size distribution can be quantified by the characteristic size (defined as the mean size). In this thesis we will test the sensitivity of the rate of aggregation on the broadness of the size spectrum.

Current Numerical Weather Prediction (NWP) models use parameterization schemes for ice phase processes, because the grid spacing of NWP models, (~20 km) cannot explicitly resolve the ice microphysics. The parameterization of aggregation quantifies the rate of change in the mixing ratio of snow aggregates arising from collection of ice crystals. Aggregation parameterization schemes utilized in NWP models do not distinguish between the different ice crystal shapes, despite the fact that observations and theory suggest that the collection process depends on the shape of ice crystals. These microphysical processes are an integral part in the parameterization of aggregation. Thus, the exclusion of ice crystal shape results in an inaccurate representation of the collection rate over a range of temperatures, because the different fall velocities of ice crystals are neglected and the rate of mass growth does not change.

1.4 Statement of Research Objectives

This thesis has two main objectives. The first objective is to develop a computationally efficient numerical parameterization scheme of the snow aggregation process that includes the major effects of different ice crystal shapes. In particular, we will formulate an aggregation scheme that can be used for plate-like crystals (for warmer temperatures) and dendrites (for colder temperatures). The local air temperature

will be the major factor in determining the shape of the ice crystals and their interactions with each other. The second objective of this thesis is to determine the relative importance of the snow aggregate size distribution on the collection rate.

To investigate the effects of cloud ice crystal shape, we will deal with the following questions: (i) how do ice crystal shapes affect their mass, cross-sectional area when falling, terminal fall velocity, and the rate of mass growth? (ii) how does the rate of snow aggregation depend on the broadness of a size distribution of ice crystals and snow aggregates?

1.5 Organization of thesis

In Chapter 2, we provide background information on individual ice crystals. Specifically, we review the classification of different ice crystal habits and provide formulae that relates ice crystal geometries with the crystals' mass, cross sectional area, terminal fall speeds, and collection efficiencies. Much of this chapter is a review of material found in typical textbooks on ice microphysics. In Chapter 3 an analytic expression is developed for the parameterization of ice aggregation. The role of a snow aggregate's size distribution in the parameterization is described. The control case for both the size distribution and collection rate is defined. Chapter 4 discusses the effect of ice particle shape on the collection rate from cloud ice crystals to snow aggregates. This is done by comparing the change in collection rate with temperature and isolating the effect of ice crystal shape on the collection rate. In Chapter 5 we examine the effect of different snow aggregate size distributions on the collection rate. Chapter 6 looks at the fractional rate of increase of mass of the different ice crystal shapes and compares them to the fractional rate of increase of mass by diffusion.

2. MICROPHYSICAL EQUATIONS FOR ICE AGGREGATION

2.1 Shapes of ice crystals

Ice crystals develop into a number of shapes, each of which displays a distinctive hexagonal characteristic. The most common shapes are: columns – long, narrow prisms of hexagonal cross section; plates – thin, solid plates having six sides; and dendrites – six-sided stars, with each arm typically having intricate, branched structures (see Figure 1.1).

The hexagonal shapes are a result of the molecular structure of a water molecule. A water molecule is made up of one oxygen atom and two hydrogen atoms. Each atom is made up of electrons with negative charge surrounding protons with positive charge. The geometrical distribution of these charges in the water molecule is such that on the side of the water molecule where the hydrogen atoms are attached there is slightly more positive charge than negative charge; conversely on the oxygen atom side of the water molecule there is a slightly more negative charge. Because of this charge distribution, water is a polar molecule. When two water molecules approach, the positive side of the one will be attracted to the negative side of the others. In the solid or ice phase, water molecules are tightly bonded to each other in a regular crystal lattice. The geometry of the lattice comes from the polar molecular structure of the hexagonal shape. The resultant bond between neighboring water molecules is very strong, consequently the heat of sublimation (forming water vapor) is large.

There are numerous observational studies that indicate ice crystal shape depends on ambient environmental conditions, primarily on local air temperature (see Figure 1.2). The dashed-dotted curve in Figure 1.2 gives the excess vapor density over ice equilibrium in an atmosphere saturated with respect to water for typical nimbus cloud conditions. The figure indicates the excess vapor density is a maximum at about -15°C. The preferred crystal types in the -15°C region are seen to be dendrites and sector plates. As a growing crystal moves through a cloud, its crystal habit will change according to the changing ambient temperature.

Hallet (1984) reported measurements that suggest most ice crystals in snow-producing clouds have planar structures for warmer temperatures, while dendrites form

the majority of ice crystals for temperatures colder than -12°C. Based on these findings, we make the simplifying assumption that snowflakes produced in temperatures ≤ -12°C are aggregates of dendrites, while for temperatures ≥ -8°C snowflakes are aggregates consisting of plates. For the intermediate temperature range, a mixture of plates and dendrites form the snowflake.

2.2 Mass of ice crystals and snow aggregates

The mass and size of different forms of ice crystals are typically related by formulas of the form $M_i = aD_i^b$ where M_i is mass (g) and D_i is the major linear dimension (cm) of the crystal. The values of a and b depend on ice crystal shape. Houghton (1985) and Rogers and Yau (1989, p. 165) give

$$M_i = 0.019\, D_i^3 \qquad \text{for plates,} \tag{1}$$

$$M_i = 0.00038\, D_i^2 \qquad \text{for dendrites.} \tag{2}$$

The subscript i denotes individual ice crystals. Note that the mass depends on the square of the linear dimension for dendrites, compared to the cube of the linear dimension for plates. As we will see later, this will have a significant impact on the relative growth rate of plates versus dendrites.

While there are many empirical studies relating individual ice crystal size with crystal mass, we are unaware of any published relationship between the mass of a snow aggregate and the spatial dimension of the snow aggregate. In other words, we are lacking a M_a - D_a relationship, where M_a denotes the mass of a snow aggregate (g), and D_a is the major linear dimension of the snow aggregate (cm). The assumption used in this work is that when air temperatures warmer than or equal to -8° C, snow aggregates consists mainly of plate-like crystals and that the M_a - D_a relationship of the snow aggregate mimics that of individual plates. We further assume that for air temperatures colder than or equal to -12° C, snow aggregates consist mainly of dendritic crystals. As a result,

$$M_a = 0.019\, D_a^3 \qquad \text{for } T \geq -8^\circ\text{C}, \tag{3}$$

$$M_a = 0.00038\, D_a^{\,2} \quad \text{for } T \leq -12^{\circ}\,C. \tag{4}$$

For air temperature values within -8° C to - 12° C, we assume a simple linear interpolation between the *a* and *b* values listed above. For example,

$$M_a = \frac{(0.019 + 0.0038)}{2} D_a^{\,(3+2)/2} \qquad \text{for } T = -10^{\circ}\,C.$$

2.3 *Terminal fall velocities of ice crystals and snow aggregates*

Consider a snow aggregate of mass M_a and major dimension D_a falling through the atmosphere. The aggregate reaches its *terminal fall speed* when a balance between the gravitational force and the drag force exerted on the falling aggregate is reached. The gravitational force is given by

$$F_{gravity} = M_a\, g\,,$$

where g is the gravitational acceleration. In the viscous flow regime, the drag forces are given by (e.g. Roger and Yau 1989, p. 124)

$$F_{drag} = \frac{1}{2} V_a^{\,2}\, A_a\, \rho\, C_{drag}\,,$$

where V_a is the fall velocity of the aggregate relative to the air, A_a is the cross-sectional area of the aggregate, ρ is the density of air, and C_{drag} is the drag coefficient characterizing the crystal. Ice crystals tend to fall with the major axis in the horizontal plane under steady conditions (Sasyo, 1971). According to Cotton *et al.* (1986) the effective cross-sectional area for plate and dendrite shaped aggregates is given by

$$A_a = \frac{\pi}{4}(D_a + D_i)^2\,, \tag{5}$$

where D_a and D_i are the major aggregate and crystal dimensions. In principle we could relate the terminal fall velocity V_a with the crystal's mass M_a by assuming an appropriate drag coefficient and equating the two forces. However, finding an accurate expression of the drag coefficient for different crystal shapes is very complicated, and it is convenient to use an empirical V_a - D_a relationships based on laboratory experiments.

In this thesis we use (V_i - D_i) and (V_a - D_a) fall velocity equations that combine the experimental works of Langleben (1954), Mason (1971), Houghton (1985) and

Khain and Sednev (1995) (see Appendix B for details). Using the ice crystal mass of different shapes, given by Mason (1971) and Houghton (1985), and the density of Khain and Sednev (1995), an ice crystal's diameter is related to the spherical diameter of the drop formed when it is melted. The equation relating the two diameters is substituted in the fall velocity of Langleben (1954) to yield:

$$V_i = c(D_i)^d \left(\frac{\rho_o}{\rho}\right)^{1/2}, \tag{6}$$

$$V_a = c(D_a)^d \left(\frac{\rho_o}{\rho}\right)^{1/2}, \tag{7}$$

where V_i, and V_a are in cm s^{-1}, D_i and D_a are in cm, 'c' and 'd' are given in Table 2.1, ρ is air density (g cm^{-3}), and ρ_o is surface air density (g cm^{-3}). The square root of air densities accounts for the increasing fall velocity with increasing altitude (Lin *et al.*, 1983).

Table 2.1 Fall velocity parameters as a function of air temperature.

Temperature	*c*	*d*
T ≥ -8 ° C	169.7	0.300
T= -9° C	147.8	0.284
T= -10° C	125.8	0.269
T= -11° C	103.9	0.253
T ≤ -12 ° C	81.9	0.237

Figure 2.1 depicts the functional relationship between terminal fall velocity and size of an ice crystal or snow aggregate. The results indicate that the terminal fall speed increases monotonically as the size of the hydrometeor increases. For a given size, a plate-like crystal falls faster than a dendrite. A dendrite's terminal fall speed ranges from about 30 cm s^{-1} to 90 cm s^{-1}, whereas a plate's terminal falls speed ranges from about 50 cm s^{-1} to 200 cm s^{-1}.

The novelty of our work is that it allows for a variable terminal fall velocity of ice crystals and snow aggregates based on the air temperature. This differs from previous studies that formulated a parameterization scheme for snow aggregation, which have adopted a terminal fall velocity that was uniform for different temperatures. Lin *et al.* (1983) utilized the fall velocity equation of Locatelli and Hobbs' (1974) for all ice

crystals at all temperatures. This method, however, was restricted to snow aggregates with diameters of 0.05 to 0.22 cm. It is commonplace to find snow aggregates that exceed these dimensions, thus the fall velocity equation of Locatelli and Hobbs is deemed insufficient. Cotton *et al.* (1986) used an ice crystal fall velocity (V_i) of hexagonal plates from Hobbs *et al.* (1972) and an aggregate fall velocity (V_a) of their own. Cotton *et al.* (1986) did not place a diameter restriction on their calculations of fall velocity and their fall velocities range from 50 to 150 cm s^{-1}. This is considered too high for dendritic snow aggregates when compared to the observations of Nakaya and Terada (Rogers and Yau, 1989, p.164).

2.4 Mass growth of a snow aggregate by collection of ice crystals

Collisions between ice crystals and snow aggregates occur due to the differential responses of crystals and aggregates to gravitational and aerodynamic/turbulent forces. Gravitational forces cause larger crystals (or aggregates) to fall faster than smaller crystals, overtaking and capturing a fraction of those lying in their path. Differential responses to aerodynamic forces (i.e. air turbulence) tend to increase the sweep-out volume marginally. As an aggregate falls, it collides with only a fraction of the crystals in its sweep-out path because crystals can be swept aside in the air stream around the aggregate. The probability of collision, called the collision efficiency, is the ratio of the actual number of collisions to the number of ice crystals in the sweep-out path. In ice microphysics it is usually assumed that the collision efficiency is close to 100%, this means that all ice crystals in the collector crystal's path are involved in actual collisions.

Collision, however, does not guarantee adhesion. Upon collision two crystals may simply bounce apart instead of sticking together. The ratio of the number of coalescences to the number of collisions is called the coalescence efficiency. Laboratory experiments of colliding ice crystals indicate that the coalescence efficiency of ice crystals is typically less than 100%. This complicates the aggregation process of ice crystals and must be accounted for. The fraction of ice crystals which collide and adhere to the collector ice crystal as it sweeps out a volume of air is called the collection efficiency.

To illustrate the effects of the cross-sectional area, fall velocity, the mixing ratio of cloud ice crystals, and collection efficiency, as mentioned above, on the formation of a snow aggregate's mass growth rate, consider a large ice crystal, of diameter D_a and fall velocity V_a, falling through a population of background cloud ice crystals of diameter D_i and fall velocity V_i. If the fall velocities, V_a and V_i, are identical, the two ice particles will not collide; however, if there is a differential response in fall velocity (δV) the ice particles may interact (δV is defined in Section 2.5). During a unit of time the snow aggregate sweeps out ice crystals from a volume given by

$$\frac{\pi}{4}(D_a + D_i)^2 |V_a - V_i + \delta V|.$$

Thus the average number of ice crystals collected in unit time is given by

$$\frac{\pi}{4}(D_a + D_i)^2 |V_a - V_i + \delta V| N E,$$

where N denotes the number of ice crystals per unit volume and E denotes the collection efficiency, which is the product of collision efficiency and coalescence efficiency. The total rate of increase of mass of the snow aggregate is given by

$$\frac{dM}{dt} = \frac{\pi}{4}(D_a + D_i)^2 |V_a - V_i + \delta V| E r_i \rho, \qquad (8)$$

where r_i is the ice mixing ratio (g g^{-1}) and δV the differential response velocity (cm s^{-1}). Equation (8) captures the principle of conservation of mass of ice (Rogers and Yau, 1989, p. 166).

2.5 Expected differential fall velocity

In contrast to hailstones whose terminal fall velocity depends greatly on size, covering a range up to 50 m s^{-1}, ice crystals tend to have rather similar terminal fall velocities close to 75 cm s^{-1}. This similarity in fall velocity decreases the probability of collisions between ice crystals of the same shape. It should be noted, however, that different-sized ice crystals react to atmospheric velocity fluctuations in dissimilar manners as a result of different inertia. Larger ice crystals or snow aggregates tend to take longer to react to atmospheric turbulent fluctuations compared to smaller ice crystals. This difference in inertial response results in a variation in fall velocities,

increasing the probability of collisions among ice crystals. The inertial response for smaller ice crystals is a greater fraction of their fall velocity than larger ice particles, thereby increasing the differential fall velocity of smaller crystals more than larger crystals. This in turn increases collisions amongst smaller crystals more than large crystals. To account for the effects of differing inertial responses on the mass growth rate we have added the term δV (in equation 8). What is an appropriate magnitude for δV?

Böhm (1992) derived a theoretical expression to quantify the expected differential fall velocity

$$V_E \equiv |V_a - V_i| + \delta V \,. \tag{9}$$

$$V_E = V_a F\left(\frac{V_a}{V_i}\right) + V_i F\left(\frac{V_i}{V_a}\right), \tag{10}$$

Where $$F(z) = \varphi\left(\frac{\ln z + \sigma^2}{2\sigma}\right),$$

$$\varphi(z) = 2\pi^{-1/2} \int_0^z e^{-t^2} dt \equiv \tanh\left(\frac{2z}{\pi^{-1/2}} + 0.1012 z^3\right),$$

therefore,

$$V_E = V_a \tanh\left\{2\pi^{-1/2}\left(\frac{\ln\left(V_a/V_i\right) + \sigma^2}{2\sigma}\right) + 0.1012\left(\frac{\ln\left(V_a/V_i\right) + \sigma^2}{2\sigma}\right)^3\right\} +$$

$$V_i \tanh\left\{2\pi^{-1/2}\left(\frac{\ln\left(V_i/V_a\right) + \sigma^2}{2\sigma}\right) + 0.1012\left(\frac{\ln\left(V_i/V_a\right) + \sigma^2}{2\sigma}\right)^3\right\}.$$

V_E represents the expected differential velocity (in cm s^{-1}), and σ represents the standard deviation. Böhm (1992) argued that $\sigma = 0.25$ for cloudy air. Using this value and typical ice crystal sizes, we find that the value of δV ranges from about 0.5 to

5 cm s^{-1}. Comparing the values of 0.5 to 5 cm s^{-1} indicates δV = 2 cm s^{-1} best represents the changes in δV of small crystals, without compromising the accuracy of δV of large snow aggregates.

2.6 Collection efficiency

The collection efficiency (E) is a measure of the fraction of cloud ice crystals which collide and adhere to a snow aggregate as it sweeps out a volume of air. The collection efficiency is the product of the collision efficiency and coalescence efficiency. Hosler *et al.* (1957), Hallgren and Hosler (1960), and Hosler and Hallgren (1960) reported laboratory experiments that indicated that the collection efficiency increased with increasing temperature, reaching a maximum at 0°C. They attributed this finding to the dependence of coalescence on the existence of a liquid film on the ice crystal's surface. A liquid film exists on the surface of ice crystals a few degrees below 0°C and upon contact with another ice crystal the two films unite and freeze acting as a bond between the ice particles. The film's thickness has been shown to be optimal for bonding at temperatures slightly below freezing (up to 0.04 μm).

There have been two main schools of thought when it comes to studying ice crystal–ice crystal collection efficiencies. One school observes free falling snow crystals in nature (Rogers, 1974, Passarelli, 1978); the other school induces interactions between small crystals and large, fixed spherical ice targets in laboratory experiments (Hosler *et al.*, 1957, Hallgren and Hosler, 1960, and Hosler and Hallgren, 1960). These studies are the basis of assumptions made in models of aggregation.

2.6.1 Comparison of collection efficiencies from Cotton et al. (1986) and Lin et al. (1983)

The collection efficiency of Cotton *et al.* (1986), shown in Figure 2.2, is composed of two parts. The first part, which applies to all temperatures except -15 through -12°C, is a linear approximation of data from Hallgren and Hosler (1960) denoted by the formula $E = min(0.2, 10^{0.035\,Ta - 0.7})$ where T_a, assumed equivalent to T in our calculations, is in degrees Celsius. The linear approximation of Hallgren and

Hosler's (1960) data reaches a conservative maximum of 20%. The collection efficiency of Hallgren and Hosler (1960), however, should have been doubled because their discussion clearly states the use of an average cross-sectional area is approximately double that in reality and underestimated the collection efficiency by half. In reality, only half the area is actually occupied by ice and the other half by holes. Consequently, the linear approximation assumed by Cotton *et al.* (1986) was half what it should be. Part two of Cotton *et al.*'s (1986) collection efficiency, which applies to the temperatures -15 through -12°C, is set as 140% following Passarelli (1978). Passarelli (1978) used aircraft and Doplar radar measurements of snow-size spectra and a model of the stochastic collection process to determine the height evolution of a snow-size spectrum. From the height evolution of the snow-size spectrum the mean collection efficiency of snowflakes is estimated. Passarelli (1978) concluded dendritic aggregates, in the temperature range of -15 to -12°C, have an estimated mean collection efficiency of 140% $\pm$ 60%. Passarelli (1978) lists three possible causes for the collection efficiency surpassing unity: wake capture, horizontal motion of the ice crystals (thereby increasing the sweep out volume), and a spectrum of fall speeds for snow aggregates of the same mass (the dispersion in fall speeds enhances aggregation).

Cotton *et al.* (1986) made a relative comparison of three collection efficiencies: (i) a control case with the collection efficiency as outlined above; (ii) with the collection efficiency equal to the linear approximation of Hallgren and Hosler's (1960) data; and (iii) with a collection efficiency equal to 140% for temperatures warmer than -16°C. For case (i) the mixing ratio of snow aggregates reached a maximum of 0.23 g kg^{-1} near the surface, whereas in case (ii) the peak snow aggregate mixing ratio was 0.07 g kg^{-1} as a result of the reduced aggregation at colder temperatures. For case (iii) the greater collection efficiency increased aggregation such that the maximum snow aggregate mixing ratio was 0.37g kg^{-1}. The reduced aggregation in case (ii) resulted in an approximate reduction of 25% in the predicted precipitation – demonstrating the influence of aggregation, especially if one considers the application of such a model to orthographic cloud seeding experiments (Cotton *et al.*, 1986). Case (i), the most realistic simulation in Cotton *et al.* (1996), underestimates the observed station precipitation

amount by 46 to 48%. The cause of the under prediction in precipitation is unknown but possibly influenced by the underestimate in the aggregation model.

The collection efficiency data proposed by Lin *et al.* (1983), also shown in Figure 2.2, was calculated using $E = exp(0.025\ T)$, where T is in degrees Celsius. They assume a maximum collection efficiency of unity but did not mention a source on which they based their assumption.

2.6.2 *Collection efficiency from experimental data*

From observations of free-falling snow and a non-depleting model of ice aggregation, Rogers (1974) calculated a collection efficiency ranging from 0.1 to 0.6. Rogers' (1974) collection efficiency is the basis of Khain and Sednev's (1996) collection efficiency equation although this type of model underestimates the collection efficiency (Passarelli, 1978). As Rogers' (1974) collection efficiency is the only one based on free falling snow it is used in our research. Using experimental data from Hosler *et al.* (1957), Khain and Sednev (1996) developed a collection efficiency equation that is not solely dependent on temperature but also includes the atmospheric vapour pressure over ice. Khain and Sednev (1996) showed that as temperature approaches 0°C, the collection efficiency of colliding ice particles will approach the collection efficiency of colliding drops. The collection efficiency of colliding ice particles, however, never exceeded the collection efficiency of colliding drops. Hall (1980) demonstrated that drops greater than 100 μm collecting background drops greater than 50 μm have a collision efficiency of 100% and assuming a coalescence efficiency of unity, the collection efficiency of drops is 100%. The collection efficiency (E) of Khain and Sednev (1996) assumed that the collection efficiency remains the same for all ice crystal types and is given as

$$\begin{aligned} E &= E_L \times \delta E \frac{e}{e_{si}}, && for \quad \delta E \frac{e}{e_{si}} < 1 \\ E &= E_L && for \quad \delta E \frac{e}{e_{si}} \geq 1 \end{aligned} \qquad (11)$$

where E_L represents collection efficiency of water drops and is set as 1 (Hall, 1980), e is water vapour pressure, and e_{si} is the saturated vapour pressure with respect to ice. Both δE and e/e_{si} are functions of temperature and are given as

$$\frac{e}{e_{si}} \cong \frac{e}{e_s}\left[\frac{273}{(273+T)^{2.66}}\right], \tag{12}$$

and $$\delta E = \max\left\{0, 0.883 + (0.093\mathrm{T}) + (0.00348\,\mathrm{T}^2) + (0.000045185\,\mathrm{T}^3)\right\} \tag{13}$$

where T is in °C (Rogers and Yau, 1989, p. 15 & 16 and Khain and Sednev, 1996 respectively). The variable e_s represents the saturated vapour pressure and $e/e_s \times 100$ = *Relative Humidity*. The collection efficiency of Khain and Sednev (1996) is compared to those of Lin *et al.* (1983) and Cotton *et al.* (1986) in Figure 2.2.

2.7 Summary

In this chapter, the ice crystal classification by Kobayashi (1958) was simplified into four ice crystal shapes: columns, plates, sector plates, and dendrites. The latter three are the only ice crystal shapes considered in our research. We assume that aggregation is only permitted between ice crystals of the same shape, i.e. plates collect plates and dendrites collect dendrites, and the resulting snow aggregates are of the same shape as the colliding ice crystals.

The mass growth rate of an ice crystal by aggregation is a function of three factors contributing to the collision of ice particles and one factor affecting adhesion: the expected differential fall velocities of ice particles, the cross-sectional area of ice particles, the mixing ratio of cloud ice crystals; and the collection efficiency, respectively. The mass growth rate is calculated by:

$$\frac{dM}{dt} = \frac{\pi}{4}(D_a + D_i)^2 \left|V_a - V_i + \delta V\right| E\, r_i\, \rho\,. \qquad \text{(equation 8)}$$

To understand the expected differential fall velocity, the fall velocity of ice crystals and snow aggregates must be first understood. In this chapter a simple fall velocity equation was developed to represent all three ice crystal shapes and sizes because the single fall velocity in Lin *et al.* (1983) and Cotton *et al.* (1986) is deficient in representing all the different ice crystal shapes. The fall velocity of the ice crystals

from fastest to slowest are: plates, sector plates, and dendrites. Now, falling ice crystals collide with other ice crystals in their path if there is a difference between their fall velocities. Ice crystals of the same shape have similar fall velocities despite differences in size. This decreases the probability of collisions between ice crystals of the same shape but the different reactions to turbulence by different-sized ice crystals causes a differential fall velocity. Larger ice crystals take longer to react to atmospheric fluctuations compared to smaller ice crystals, so to account for this an expected fall velocity is used.

The cross-sectional area of plates, sector plates, and dendrites are assumed to equal the area of a circle with a diameter equal the sum of the collector and collected crystals diameters. By neglecting columnar ice crystals there is no need to change the equation for the cross sectional area. The greater the cross-sectional area, the more ice crystals a snow aggregate intercepts.

The collection efficiency is a measure of the ice crystals which collide and adhere to a snow aggregate as it sweeps out a volume of air. The collection efficiency is a function of a film on an ice crystal's surface which freezes and acts like a bond between two ice crystals upon contact. The film's thickness, and hence the collection efficiency, is optimal at 0°C. The collection efficiencies in Lin *et al.* (1983) and Cotton *et al.* (1986), which are both solely functions of temperature, are unsatisfactory. The collection efficiency in Khain and Sednev (1996) is selected and it is a function of temperature and relative humidity.

The mass growth rate of dendrites is slower than that of plates, of equal diameter, because: (i) dendrites have a smaller fall velocity; and (ii) dendrites occur in cooler temperatures than plates so the collection efficiency of dendrites is lower.

3. PARAMETERIZATION OF ICE AGGREGATION

3.1 Snow aggregate size distribution

Ice aggregation in bulk-water parameterization schemes is represented as the integration of the mass growth of a single aggregate over the entire snow aggregate size distribution. The total rate of ice aggregation is denoted by $C = \frac{dr_a}{dt}$ (g g^{-1} s^{-1}) and given by

$$C = \int_0^\infty \frac{1}{\rho} \frac{dM}{dt} N(D_a)\, dD_a, \tag{14}$$

where D_a denotes the effective diameter of the snow aggregate and $N(D_a)\, dD_a$ denotes the number of snow aggregates of effective diameter between D_a and $D_a + dD_a$ per unit volume of air.

There are two different methods of quantifying the size spectrum of snow aggregates. One approach expresses the size of a given snow aggregate as the equivalent diameter of its melted water drop. By melting the snowflake, the diameter of the melted sphere of liquid water characterizes the amount of water mass in the snowflake. Gunn and Marshall (1958) developed this technique by collecting snow aggregates on brushed wool, melting them, and applying filter paper to the wool to absorb the drops. They then measured the number of drops collected in a given size interval, per unit time. The observed distribution were divided by Langleben's (1954) fall velocities for the snow aggregates in each size interval to determine the concentration $N(D_a)$ of snow aggregates in space (Rogers and Yau, 1989, p.181). The melted snow aggregate distribution implicitly assumes the fall velocities of snow aggregates depend solely on the mass (i.e. melted diameter). The second method of quantifying the size spectrum of snow aggregates measures the maximum dimension of collected snow aggregates which have fallen in a given time interval. Rogers (1974) argued that this method is more suited for studying the aggregation process as it is a true representation of snow aggregates.

Observations suggest that the size spectrum of snow aggregates can be approximated by an inverse exponential particle size distribution:

$$N(D_a) = N_o \exp(-\lambda_a D_a), \tag{15}$$

where N_o represents the intercept parameter of the snow size distribution, and λ_a is the slope parameter in the snow aggregate size distribution which typically depends on the snowfall rate (Figure 3.1). In theoretical studies of snowfall development it is often necessary to compute moments of the size distribution; for example, the flux of snow falling through a horizontal area (i.e. the snowfall rate), the mass of snow per unit volume (i.e. snow content), and the radar reflectivity of snow are all related to certain moments of $N(D_a)$. The inverse exponential size distribution is convenient because its moments are known analytically:

$$\int_0^\infty D_a{}^n \, N(D_a)\, dD_a = \int_0^\infty D_a{}^n \, N_o \exp(-\lambda_a D_a)\, dD_a$$

$$= N_o \, \Gamma(n+1)\, \lambda_a{}^{-(n+1)}, \tag{16}$$

where Γ denotes the gamma function (for an integer n, $\Gamma(n+1) = n!$). The analytical result (equation 16), which has an infinite upper limit of integration, is a good approximation for real distributions that have a finite upper limit of diameter. The exponential form of $N(D_a)$ falls off rapidly with D_a such that unrealistically large particles implied by the infinite limit make little contribution to the integral (Rogers and Yau, 1989, p.181).

Substituting equation 15 into equation 14, and using knowledge of equation 16, leads to the general solution for the collection rate (C) (Appendix C):

$$C = \frac{\pi}{4} E \, r_i \, N_o \left[\begin{array}{l} c\left(\frac{\rho_o}{\rho}\right)^{0.5} \Gamma(3+d)\, \lambda_a{}^{-(3+d)} + 2cD_i \left(\frac{\rho_o}{\rho}\right)^{0.5} \Gamma(2+d) \lambda_a{}^{-(2+d)} \\ + cD_i{}^2 \left(\frac{\rho_o}{\rho}\right)^{0.5} \Gamma(1+d) \lambda_a{}^{-(1+d)} + \left(\delta V - cD_i{}^d \left(\frac{\rho_o}{\rho}\right)^{0.5} \right) \Gamma(3)\, \lambda_a{}^{-3} \\ + \left(2\,\delta V\, D_i - 2cD_i{}^{1+d} \left(\frac{\rho_o}{\rho}\right)^{0.5} \right) \Gamma(2) \lambda_a{}^{-2} + \left(\delta V\, D_i{}^2 - cD_i{}^{2+d} \left(\frac{\rho_o}{\rho}\right)^{0.5} \right) \Gamma(1) \lambda_a{}^{-1} \end{array} \right] \tag{17}$$

3.2 *Previous aggregation parameterizations*

The pioneering work on bulk-water parameterization schemes for ice phase processes was done by H. Orville at South Dakota School of Mines and Technology (Lin *et al.*, 1983) and W. Cotton at Colorado State University (Cotton *et al.*, 1986).

The South Dakota School of Mines and Technology cloud model distributes the water substance over 5 categories: water vapor, cloud water, cloud ice, rain (liquid precipitation), snow (ice precipitation), and hail/graupel. The ice aggregation process is parameterized using the following assumptions:

- The cross-sectional area (A) is related to the ice aggregate equivalent melted diameter using: $A = \frac{\pi}{4} D_{equivalent}^{\ 2}$.
- The fall velocity of all snow aggregates (V_a) is related to their equivalent melted diameter using: $V_a = 152.93\, D_{equivalent}^{\ 0.25} \left(\frac{\rho_o}{\rho}\right)^{0.5}$.
- The collection efficiency is a function of temperature:

  $E = \exp(0.025T)$, where T is temperature (°C).
- The size distribution of snow aggregates is given by the inverse exponential size distribution of Gunn and Marshall (1958):

  $$N(D_{equivalent}) = 0.03 \exp\left(-\lambda_a\ D_{equivalent}\right),$$

  where λ_a is the slope parameter in the snow aggregate size distribution.

By combining these assumptions, the rate of ice aggregation is computed as:

$$C = \frac{\pi}{4}\left(\frac{\rho_o}{\rho}\right)^{0.5} (152.93)(0.03)\, E\, r_i \frac{\Gamma(3+0.25)}{\lambda_a^{\ 3+0.25}},$$

where λ_a is given by $\lambda_a = \left(\frac{0.03\,\pi\,\rho_a}{\rho\, r_a}\right)^{0.25}$.

To close the parameterization scheme, we write C in terms of snow mixing ratio r_a rather than the slope parameter λ_a. The snow aggregate mixing ratio is related to λ_a using:

$$r_a = \frac{1}{\rho}\int_0^\infty \frac{4}{3}\pi\left(\frac{D_{equivalent}}{2}\right)^3 \rho_a\, N(D_{equivalent})\, dD_{equivalent}$$

$$= \frac{\pi}{6}\frac{\rho_a}{\rho}\int_0^\infty D_{equivalent}{}^3\, 0.03 \exp\left[-\lambda_a D_{equivalent}\right] dD_{equivalent}$$

$$= 0.03\frac{\pi}{6}\frac{\rho_a}{\rho}\frac{\Gamma(3+1)}{\lambda_a{}^4},$$

where ρ_o is surface air density (g cm^{-3}), ρ is air density (g cm^{-3}), ρ_a is snow aggregate density (0.1 g cm^{-3} in Lin *et al.* (1986)), and r_a is the mixing ratio of snow aggregates (g g^{-1}). Expressing the collection rate (C) in terms of the snow aggregate mixing ratio gives:

$$C = \frac{\pi}{4}\left(\frac{\rho_o}{\rho}\right)^{0.5}(152.93)(0.03)\,E\,r_i\,\frac{\Gamma(3.25)}{\left(\frac{0.03\pi\rho_a}{\rho\, r_a}\right)^{3.25/4}}.$$

The parameterization of aggregation in Cotton *et al.* (1986) begins with the assumption that there is an equal size cloud ice crystal population; based on Passarelli (1978), in which a distribution of fall velocities is constructed using an ice crystal's density spectrum (Cotton and Anthes, 1989, p.132). Cotton *et al.*'s (1986) model makes the following assumptions:

- The cross-sectional area is dependent on the diameters of both the snow aggregate and the (non-precipitating) small ice crystals particles: $A = \frac{\pi}{4}(D_a + D_i)^2$.
- The terminal fall velocity of the snow aggregate is given by:

$$V_a = 2.49\,\beta^{0.5}\,D_{mo}{}^{0.2}\left(\frac{9.81}{3(1.3)\rho}\right)^{0.5}, \qquad \text{where } \beta = 0.015 \text{ cm}^{-2.4}.$$

- The terminal fall velocity of ice crystals is given by

$$V_i = 304\,D_i\left(\frac{\rho_o}{\rho}\right)^{0.5}.$$

- The collection efficiency is a function of temperature given by

$$E = \begin{cases} T \neq [-15^{o}C, -12^{o}C] & \min[0.2, 10^{0.035T_a - 0.7}] \\ T = [-15^{o}C, -12^{o}C] & 1.4 \end{cases}, \quad \text{where } T_a = T \text{ (in } ^{o}\text{C)}.$$

- The snow aggregate size distribution is given by the unmelted size distribution of Rogers (1974):

$$N(D_a) = 0.641\beta^{-1}\,\rho r_a\, D_{mo}^{-3.4} \exp\left[-\frac{D_a}{D_{mo}}\right],$$

where $\beta = 0.015$ g cm$^{-2.4}$ and $D_{mo} = 0.33$ cm (Cotton *et al.*, 1986; Passarelli, 1978; Rogers,1974).

By combining these assumptions the rate of ice aggregation (C) can be computed as

$$C = \frac{0.5\rho}{\beta} E r_a r_i D_{mo}^{-2.4} |V_a - V_i| \left(2D_{mo}^{2} + 2D_i D_{mo} + D_i^{2}\right).$$

3.3 Control case

In order to determine the effects of a size distribution on the rate of ice aggregation we must quantify the "broadness" of a size distribution. To do this we select the unmelted exponential size distribution of Rogers (1974) as our control size distribution $N(D_a)$. It is given as:

$$N(D_a) = N_o \exp[-\lambda_a D_a]$$

$$N(D_a) = N_{oo}\,\rho r_a\, D_m^{-3.4} \exp\left[-\frac{D_a}{D_m}\right], \qquad (18)$$

where N_{oo} equals $0.641/\beta$ with $\beta = 0.015$ g cm$^{-2.4}$, ρ is air density (g cm^{-3}), D_m is the characteristic diameter, and r_a is mean mixing ratio of snow aggregates (g g^{-1}). Based on 28 samples of snowfall, Rogers (1974) found that the average D_m value was 0.33 cm, which we denote as D_{mo}. Combining (17) and (18) gives:

$$C = \frac{\pi}{4} E r_i N_{oo} \rho r_a D_m^{-3.4} \left[\begin{array}{l} c\left(\frac{\rho_o}{\rho}\right)^{0.5} \Gamma(3+d) D_m^{(3+d)} + 2cD_i\left(\frac{\rho_o}{\rho}\right)^{0.5} \Gamma(2+d) D_m^{(2+d)} \\ + cD_i^2\left(\frac{\rho_o}{\rho}\right)^{0.5} \Gamma(1+d) D_m^{(1+d)} + \left(\delta V - cD_i^d\left(\frac{\rho_o}{\rho}\right)^{0.5}\right) \Gamma(3) D_m^3 \\ + \left(2\delta V D_i - 2cD_i^{1+d}\left(\frac{\rho_o}{\rho}\right)^{0.5}\right) \Gamma(2) D_m^2 + \left(\delta V D_i^2 - cD_i^{2+d}\left(\frac{\rho_o}{\rho}\right)^{0.5}\right) \Gamma(1) D_m^1 \end{array} \right] \quad (19)$$

For a given mass of snow, we can change the broadness of the snow aggregate size distribution by changing D_m and N_{oo} (see equation 18). N_{oo} is the constant which relates the characteristic diameter and collection rate; it changes in order to maintain the same mass in the distribution. In the control case, the control characteristic diameter (D_{mo}) is set as 0.33 cm. Rogers (1974) reported observations of the characteristic diameters ranging from 0.13 cm to 0.92 cm and in terms of percentage this is 40% to 280%. In Chapter 5, we will use equation 19 to investigate how varying the size distributions, with characteristic diameters of *50, 75, 150, 200*, and *250* % of the control case, affects the collection rate. The relationship between the characteristic diameters and resulting size distributions and collection rates will also be quantified in Chapter 5.

Equation 19 shows that the collection rate (C) is directly proportional (1:1) to the ice crystal mixing ratio (r_i). This means, a doubling of r_i results in a doubling of C. An ice crystal mixing ratio of $r_i = 0.0005$ g g^{-1} is typical for cloudy air, and can increase to $r_i = 0.001$ g g^{-1} in deeper convection. As ice crystals increasingly aggregate to form snow, the mixing ratio of ice crystals decreases as r_a increases.

4. EFFECTS OF TEMPERATURE ON RATE OF AGGREGATION

The focus of this chapter is to investigate the effects of temperature on the rate of ice aggregation (C). Before using the collection rate to study the temperature dependence, however, we will briefly discuss the validity of our scheme. In section 4.2 we compare the geometric collection rates (collection rate with a collection efficiency of unity) of the control case with those of Lin *et al.* (1983) and Cotton *et al.* (1986). In section 4.3 we compare the collection rates of the control case with the collection rates of Lin *et al.* (1983) and Cotton *et al.* (1986). Section 4.4 combines the results of the collection rate by aggregation with the mass growth rate by diffusion to formulate a hypothesis that explains the optimal conditions required for the formation of large snow aggregates.

4.1 Verification of parameterization scheme for rate of ice aggregation

Before a parameterization scheme can be used to study a physical process such as aggregation, the parameterization scheme must first demonstrate that it can realistically simulate nature under specified conditions. Our aggregation parameterization scheme makes several assumptions in the approximation of various components of the collection process. While each component might have reasonable assumptions that lead to small uncertainties, it is not entirely clear that the collective effect of all the assumptions remains small. For this purpose, it is desirable to verify estimates of the results of the aggregation parameterization against observations. The major difficulty in comparing observations of snow formation with model estimates lies in the natural variability of precipitation. The variability in nimbus clouds is caused by temporal and spatial variability in the amounts of ice mixing ratio, snow mixing ratio, and in-cloud temperature. These fluctuations are usually not recorded, yet in the event that they were recorded it would be extremely difficult to use such measurements as accurate input variables for testing a bulk-water parameterization scheme for ice aggregation. Therefore, we should not expect this (or any other) aggregation scheme to simulate a particular observed snowfall event with all its details.

Cotton *et al.* (1986) validated their micro-physical parameterizations schemes by evaluating the total snowfall amounts at the ground between the cloud model and in-situ measurements. This approach requires the inclusion of all micro-physical parameterization schemes including ice nucleation, deposition-diffusion, auto-conversion of ice mixing ratio into snow mixing ratio, aggregation, melting, sublimation, condensation, evaporation, etc. The method allowed for a general assessment of the utility of the bulk-water parameterization schemes; however, it did not validate the accuracy of the aggregation parameterization scheme.

We were unable to find in the research literature suitable measurements of ice mixing ratio, snow mixing ratio, and temperature as input and verification parameters for testing the aggregation parameterization scheme. Thus to validate the collection rate we decided to compare our scheme with other model results. In section 4.3 our results will be inter-compared with the results obtained using the bulk-water parameterization scheme of Lin *et al.* (1983) and Cotton *et al.* (1986). Our approach, however, is so similar to theirs that reasonable agreement with their results is not a stringent test. Furthermore, the uncertainty of their parameterization schemes is basically the same as ours.

A real test for the validity of our model approach would be to have a model that employs significantly different methodology and assumptions. If models with different methodologies provide similar results there is likely evidence that we have realistically simulated nature. Khain and Sednev (1995) used the Stochastic Collection Equation to model the evolution of the entire size spectrum of ice crystals. Solving the Stochastic Collection Equation requires numerical integrations over several snow aggregate size categories. These computations are complex and require huge computational resources. A numerical experiment of Khain and Sednev (1995) simulates a population of snow aggregates falling through a cloud consisting of small ice crystals at a constant temperature of -12°C. For these conditions, the Stochastic Collection Equation yields a rate of aggregation of 3.5×10^{-7} g g^{-1}s^{-1}. The rate of aggregation in our parameterization is 4.5×10^{-7} g g^{-1}s^{-1} at -12°C. This suggests that our parameterization scheme is within 28% of Khain and Sednev (1995)'s more sophisticated model at one particular temperature value. Unfortunately, Khain and Sednev (1995) did not show results for

other temperature values. Also, we should stress that we have assumed the collection efficiency value (E) identical to Khain and Sednev (1995) and there exists uncertainty about its accuracy. It is obvious that more extensive verification is needed for different temperature values to assure that the parameterization of aggregation is accurate.

4.2 Geometric collection rate

The geometric collection rate is the collection rate obtained when the collection efficiency in equation 19 is set to unity giving,

$$C = \frac{\pi}{4} r_i \frac{0.641}{\beta} \rho r_a D_m^{-3.4} \left[\begin{array}{l} c\left(\frac{\rho_o}{\rho}\right)^{0.5} \Gamma(3+d) D_m^{(3+d)} + 2cD_i\left(\frac{\rho_o}{\rho}\right)^{0.5} \Gamma(2+d) D_m^{(2+d)} \\ + cD_i^2\left(\frac{\rho_o}{\rho}\right)^{0.5} \Gamma(1+d) D_m^{(1+d)} + \left(\delta V - cD_i^d\left(\frac{\rho_o}{\rho}\right)^{0.5}\right) \Gamma(3) D_m^3 \\ + \left(2\delta V D_i - 2cD_i^{1+d}\left(\frac{\rho_o}{\rho}\right)^{0.5}\right) \Gamma(2) D_m^2 + \left(\delta V D_i^2 - cD_i^{2+d}\left(\frac{\rho_o}{\rho}\right)^{0.5}\right) \Gamma(1) D_m^1 \end{array} \right] \quad (20)$$

Figure 4.1 shows the geometric collection rates of the control case, Lin *et al.* (1983), and Cotton *et al.* (1986) as a function of temperature. By eliminating the effects of the collection efficiency on the collection rate, the collection rates of Lin *et al.* (1983) and Cotton *et al.* (1986) do not depend on temperature because the terminal fall velocities and cross sectional areas are independent of temperature. The control case's geometric collection rate changes with temperature because of the changes in ice crystal shape and corresponding change in fall velocity (i.e. 'c' and 'd' changes with ice crystal shape, equations 6 and 7). As a result, the collection rate of dendrites is 44.2% that of plates; indicating ice crystal shape is important. The geometric collection rate of Lin *et al.* (1983) is approximately equal to that of dendrites in the control case, while the geometric collection rate of Cotton *et al.* (1986) is approximately equal to that of the control case's plates.

4.3 Comparison of collection rates

The temperature impacts ice crystal shape and thereby affects the fall velocity parameter (Figure 2.1), which in turn affects the mass growth rate and collection rate by aggregation for ice crystals and snow aggregates. As previously mentioned, Lin *et al.* (1983) chose a single fall velocity, namely the 'graupel-like snow of hexagonal type' of Locatelli and Hobbs (1974), and Cotton *et al.* (1986) chose a single generalized 'aggregate' fall velocity to represent all snow aggregates for all temperatures. This approach, however, is not realistic given that Kobayashi (1958) in Rogers and Yau, (1989, p.163) and Hallet (1984) in Cotton and Anthes, (1989, p.108) described a minimum of four cloud ice crystal shapes. Moreover, the single fall velocity employed by Lin *et al.* (1983) and Cotton *et al.* (1986) suggests that changes in collection rate with temperature are caused solely by the collection efficiency (E). Recall from Chapter 2 that the collection efficiencies of Lin *et al.* (1983), Cotton *et al.* (1986), and Khain and Sednev (1996) differ significantly. Equation 19 indicates that the collection rate is directly proportional to the collection efficiency. This implies that the collection efficiency must be studied further because it has a significant influence on the collection rate.

Figure 4.2 plots the collection rates of cloud ice crystals by snow aggregates as a function of temperature for Lin *et al.* (1983), Cotton *et al.* (1986), and the control case. The collection rates of Lin *et al.* (1983) and Cotton *et al.* (1986) change with temperature because of the collection efficiency - assuming r_i, r_a, β, ρ_o, ρ, D_{mo} and D_i remain constant. For the control case, the collection rate depends on the temperature via the collection efficiency, fall velocities, and cross-sectional area. Figure 4.2 shows that the collection rate for the control case reaches a maximum at 0°C, which agrees with Lin *et al.* (1983). The collection rate of Cotton *et al.* (1986) is based on the assumption that the collection efficiency equals 140% from -12 and -15°C (following Passarelli, 1978) causing the collection rate to reach its maximum in this temperature range. Observation and laboratory experiments by Sasyo (1971) suggest that the collection efficiency can indeed exceed 100% as a result of horizontal oscillations of large ice crystals and snow aggregates. In general, note that the collection rate based on our new parameterization

scheme is fairly close to that of Cotton *et al.*'s (1986) for temperatures cooler than 18°C. For temperatures warmer than -10°C, our collection rate exceeds both Lin *et al.*'s (1983) and Cotton *et al.*'s (1986) values. More observations are needed to determine whether our scheme is indeed better for warmer temperatures.

Comparison of the three collection rates with their corresponding geometric collection rates shows that the reduction in collection efficiency at temperatures less than -18°C causes the collection rate for the control case to be smaller than the collection rate of Cotton *et al.* (1986). In contrast, the high collection efficiency at temperatures greater than -9°C results in the collection rate of the control case being greater than Lin *et al.* (1983). This is because the geometric collection rate of the control case lies slightly above that of Lin *et al.* (1983) at temperatures below -12°C and slightly above Cotton *et al.* (1986) in temperatures warmer than -8°C (Figure 4.1).

4.4 Combining the collection rate by aggregation and mass growth rate by diffusion

In this section, the results of the control case's collection rate will be used in conjunction with the mass growth rate by aggregation and diffusion to form a hypothesis concerning the optimal conditions required for the formation of large snow aggregates. In rising air, ice crystals tend to grow by diffusion of water molecules onto ice crystals. The growth rate by diffusion reaches a maximum near -15°C (Byers, 1965, p.123). This maximum results in large individual ice crystals near -15°C with smaller ice crystals at warmer and colder temperatures. Combining mass growth rate of ice crystals by diffusion with mass growth rate by aggregation results in (Table 4.1):
(i) large/medium sized aggregates near 0°C composed of many small ice crystals;
(ii) small aggregates form from -9 to -11°C from individual medium sized ice crystals;
(iii) although the collection efficiency is minimum in cooler temperatures, from -12 to -25°C, large aggregates form from -12 to -15°C because a few large individual ice crystals adhere. This hypothesis is summarized in Table 4.1.

TABLE 4.1 The hypothesized snow aggregate size and composition, according to temperature (°C), based on the diffusional and aggregate growth.

	TERMPERATURE RANGE		
GROWTH	**0°C to -5°C**	**-5°C to -10°C**	**-10°C to -25°C**
Diffusional Growth	Small/Medium sized individual crystals	Medium sized individual crystals	Large individual crystals
Aggregation Growth	Optimal aggregation	Some aggregation	Little aggregation
RESULT	Large/Medium Aggregates composed of Small/Medium sized individual ice crystals	Smaller aggregates of Medium sized individual ice crystals	Aggregates near -12 to -15°C are large as a result of aggregation between large individual ice crystals

Thus, there are two temperature ranges where large aggregates can form. The first is near 0°C, as a result of the sheer number of small individual ice crystals which adhere together due to the maximum collection efficiency; and the second is near -15°C, where the adhesion between a few, yet large, individual crystals which grow rapidly by diffusion, form large snow aggregates. This hypothesis is consistent with the findings of Hobbs *et al.* (1974) which show snow aggregates are largest, and occur most frequently, near 0°C. Although both the maximum dimension and probability of occurrence of snow aggregates decreases with decreasing temperature, they both exhibit a local maximum near the dendrite growth region (near -15°C). Yeh *et al.* (1986) also confirmed the two temperature zones of large snow aggregates in clouds, one zone between 0 and -4°C and the second zone from -11 to -14°C.

In the past, researchers have typically searched for a single reason for the double peak in large aggregate size. For example, Hobbs *et al.* (1974) and Rogers and Yau (1989, p.165) believe dendrites are more likely to adhere and form larger aggregates; and Hosler and Hallgren (1960) reported that aggregation reached a maximum near -10°C despite the maximum collection efficiency at 0°C.

4.5 Summary

We examined the effects of temperature on the rate of ice aggregation. Combining the effects of temperature on the fall velocity and collection efficiency results in a collection rate that spans nearly two orders of magnitudes. The collection rate at cold temperatures is small because of relatively slow fall velocities and low collection efficiency.

We formulated a hypothesis that is consistent with observations that suggest snow is most commonly formed in two temperature zones: near 0°C (maximum aggregation) and near -12 to -15°C (maximum diffusion). This hypothesis corroborates with the findings of Hobbs *et al.* (1974) and Yeh *et al.* (1986).

5. EFFECTS OF SNOW AGGREGATE SIZE DISTRIBUTION ON COLLECTION RATE

In the previous chapter we considered the effects of temperature on the rate of aggregation. In this chapter, our focus turns to the effects of the snow aggregate size distribution on the rate of aggregation.

5.1 Effects of snow aggregate size distribution on the collection rate

The effects of the snow aggregate size distribution on the collection rate is determined by comparing the rates of aggregation (C) with size distributions with the same total mass of snow, but differing in the number of particles per size category (i.e. different distribution broadness). The total mass of the size distribution is assumed to equal the size distribution used in the collection rate for the control case (Chapter 3) which is given by

$$N(D_a) = N_{oo}\ \rho\ r_a\ D_{mo}^{-3.4} \exp\left[-\frac{D_a}{D_{mo}}\right],$$

with characteristic diameter (D_{mo}) equal to 0.33 cm and corresponding $N_{oo} = 0.641/\beta$, where $\beta = 0.015$ g cm$^{-2.4}$. Given that the broadness of a distribution is primarily governed by the characteristic diameter, size distributions with characteristic diameters equal to 50, 75, 100, 150, 200, and 250% of D_{mo} will be compared (Table 5.1).

Figure 5.1 compares the snow aggregate size distributions for characteristic diameters ranging from 0.165 to 0.825 cm. An increase in characteristic diameter broadens the distribution (i.e. decreases the number of small ice particles and increases the number of large ice particles). Large ice crystals are more likely to collide with other ice crystals and as a result, the broadest size distributions have the fastest collection rates (Figure 5.2). The collection rate increases monotonically as the characteristic diameter increases across all temperature ranges. These collection rates, with characteristic diameter values equal to 50, 75, 100, 150, 200, and 250% of D_{mo} = 0.33cm, span two orders of magnitude (10^{-8} to 10^{-6} g g^{-1}s^{-1}).

Table 5.1 **Aggregation rates as a function of characteristic diameter (D_m) for selected temperatures. The values are expressed as a ratio of $C(D_m) / C(D_{m0}) = C / C_0$.**

D_m (cm)	D_m / D_{m0}	C/C_0 T= -5 °C	C/C_0 T= -10 °C	C/C_0 T= -15 °C
0.165	50%	19.4%	19.7%	20.0%
0.248	75%	50.9%	51.2%	51.6%
0.330	100%	100%	100%	100%
0.495	150%	261%	258%	255%
0.660	200%	512%	504%	495%
0.825	250%	866%	847%	827%

The ratios of $C(D_m) / C(D_{mo})$ are listed in Table 5.1. For D_m less than $D_{mo} = 0.33$ cm, the values of C / C_0 increases with decreasing temperature. In contrast, for D_m greater than $D_{mo} = 0.33$ cm, C / C_0 increases with increasing temperature. This suggests that the presence of a broader ice crystal distribution enhances aggregation, particularly for temperatures warmer than -5°C. The characteristic diameter has a greater impact on the collection rate in warmer temperatures, which is related to the increase of collection efficiency with warmer temperatures.

5.2 Duration of snow formation

Radar observations suggest that precipitation-size particles can form within about 30 minutes. We are interested in establishing whether snow flakes can be formed within this time span based on our bulk-water parameterization scheme for aggregation. A convenient way to quantify the duration of snow formation is to use the so-called doubling-time of snow aggregates. Consider cloudy air with the following parameters: mixing ratio of snow aggregates (r_a), mixing ratio of small ice crystals or cloud ice mixing ratio (r_i), and temperature (T). Making the assumption that the size distribution of snow aggregates is the negative-exponential function (equation 18) with a characteristic diameter of D_{mo}, then the evolution of r_a assuming aggregation can be written as:

$$\frac{dr_a}{dt} = C(r_i, r_a, T, D_m) ,$$

where C is the rate of ice aggregation. Since C is proportional to r_i and r_a (equation 20) it follows that

$$\frac{dr_a}{dt} = C'(T, D_m)\, r_a\, r_i \tag{21}$$

where $C'(T, D_m)$ depends on only T and D_m but not on r_a nor r_i (see Appendix C for details). Equation (21) suggests that for fixed values of T, D_m, and r_i the mixing ratio of snow aggregates increases exponentially:

$$r_a(t) = r_a(t_o)\exp(C'(T, D_m)\, r_i\, t),$$

where $t = t_0$ denotes the initial time. For exponential growth it is convenient to introduce the *Doubling Time* (τ) defined as the time interval during which the snow mixing ratio r_a doubles in value:

$$r_a(\tau) = 2\, r_a(t_o) = r_a(t_o)\exp(C'(T, D_m)\, r_i\, \tau)$$

$$\tau = \frac{\ln 2}{C'(T, D_m)\, r_i} \tag{22}$$

Appendix D gives the equations for computing the doubling time τ. It depends on T, D_m, and r_i (but not on r_a).

Figure 5.3 shows curves of τ plotted against temperature (T), and Table 5.2 gives the τ at -15, -10, and -5°C, for different values of D_m/D_{mo}. As in Figure 5.2, the values of D_m/D_{mo} are labeled in percentage with D_{mo} = 0.33 cm being the characteristic diameter of the control case. The τ –T curves plotted in Figure 5.3 are based on the ice crystal mixing ratio $r_i = 5 \times 10^{-4}$ g g^{-1}. This is the typical concentration of cloud ice in snow producing clouds. For temperatures warmer than -12°C, the doubling time τ is less than 1 hour. At temperatures warmer than -25°C, only size distributions with $D_m > D_{mo}$ have doubling times less than 60 min. For the control case a doubling time below 60 min exists at temperatures warmer than -23°C, and is fastest at 0°C when the doubling time is 1.35 min. Figure 5.3 and Table 5.2 both reiterate that aggregation is fastest for broader snow aggregate size distributions. Furthermore, aggregation is faster for warmer temperatures.

Equation (22) shows that τ is inversely proportional to r_i (i.e. a doubling in r_i results in dividing τ in half). Thus the greater r_i (i.e. the more ice crystals available for collision and adhesion), the faster snow aggregates form.

Table 5.2 Doubling Times (τ) as a function of characteristic diameter (D_m) for selected temperatures.

D_m (cm)	D_m / D_{m0}	τ (min) T= -5 °C	τ (min) T= -10 °C	τ (min) T= -15 °C
0.165	50%	12	30	95
0.248	75%	4	12	38
0.330	100%	2	6	19
0.495	150%	0.85	2.5	8
0.660	200%	0.45	1	4
0.825	250%	0.25	0.70	2.5

5.3 Summary

In this chapter, the effect of snow aggregate distributions on the collection rate was investigated. This was achieved by calculating the collection rate using distributions of the same mass but varying in broadness. A size distribution is largely governed by its characteristic diameter. Rogers (1974) observed an average characteristic diameter equal to 0.33cm, which Cotton *et al.* (1986) adopted in their size distribution. The snow aggregate size distribution of Cotton *et al.* (1986) is selected as our control case. Rogers (1974) also observed characteristic diameters ranging from *40.8* to *278.0%* of the average D_m = 0.33 cm, so we varied the broadness of our distributions using characteristic diameters equivalent to 50, 75, 100, 150, 200, and 250% of the control characteristic diameter. Snow aggregate size distributions with large characteristic diameters have broader distributions because they contain more large crystals. Larger ice crystals are more conducive to aggregation and, as a result, the collection rates of broader size distributions are faster than collection rates with narrower distributions (i.e. smaller D_m). Specifically, a 50 to 250% change in the characteristic diameter corresponds to a 20 to 850% change in the collection rate (C) respectively.

The doubling time (τ), time required for the aggregate mixing ratio to double, is similar to the control collection rate in that (i) size distributions with greater characteristic diameters have short τ; and (ii) τ increases with decreasing temperature. For the size distribution with D_m = 0.33cm τ is less than 60 min for temperatures less than -23°C. Otherwise τ is less than 60 min for all size distributions for temperatures less than -12°C, or for size distributions with characteristic diameters greater than 0.33 cm.

6. GROWTH BY ICE AGGREGATION VERSUS DEPOSITION-DIFFUSION

At the initial stages of snow formation, the contribution of ice aggregation is small due to the small cross-sectional area of falling ice crystals. It is here that diffusional growth by deposition of ice on existing crystals is important. The deposition-diffusion process is more effective for ice crystals than the condensation-diffusion process for water droplets, because the vapor in the cloud is often at equilibrium relative to water and hence supersaturated with respect to ice. Light precipitation can occur in the form of individual ice crystals, indicating that aggregation never occurred. It is thus of interest to compare the relative importance of ice aggregation versus deposition-diffusion at the initial stages of precipitation formation (Rogers and Yau, 1989, p.168).

6.1 *Fractional rate of increase of mass due to ice aggregation*

The fractional rate of increase of mass (FRIM), defined as FRIM = $\frac{1}{m}\frac{dm}{dt}$, can be calculated by substituting in the equations of mass (1 through 4). For plates growing at -5°C we have:

$$\frac{1}{m}\frac{dm}{dt} = \frac{1}{0.019 D_a^{\,3}} A(D_a) \left| V_a - V_i + \delta V \right| E\, r_i\, \rho \qquad (23)$$

$$= \left(\frac{1}{0.019\, D_a^{\,3}} \right) D_a^{\,2} \left(169.7 \left(D_a^{\,0.3} - D_i^{\,0.3} \right) \left(\frac{\rho_o}{\rho} \right)^{1/2} + \delta V \right) E\, r_i\, \rho$$

$$= \frac{1}{0.019\, D_a} E\, r_i\, \rho \left(169.7 \left(D_a^{\,0.3} - D_i^{\,0.3} \right) \left(\frac{\rho_o}{\rho} \right)^{1/2} + \delta V \right)$$

For dendrites growing at -15°C we have:

$$\frac{1}{m}\frac{dm}{dt} = \frac{1}{0.00038 D_a^{\,2}} A(D_a) \left| V_a - V_i + \delta V \right| E\, r_i\, \rho \qquad (24)$$

$$= \left(\frac{1}{0.00038\, D_a^{\,2}} \right) D_a^{\,2} \left(81.9 \left(D_a^{\,0.237} - D_i^{\,0.237} \right) \left(\frac{\rho_o}{\rho} \right)^{1/2} + \delta V \right) E\, r_i\, \rho$$

$$= \frac{1}{0.00038} E r_i \rho \left(81.9 \left(D_a^{0.237} - D_i^{0.237} \right) \left(\frac{\rho_o}{\rho} \right)^{1/2} + \delta V \right)$$

The FRIM by aggregation of plates, at -5°C, and dendrites, at -15°C, are plotted in Figure 6.1. The straight lines indicate a power-law dependence of the mass growth rate on ice crystal mass. For plates at -5°C the FRIM by aggregation decreases with increasing ice crystal mass. Dendrites at -15°C have a FRIM by aggregation which, unlike that of plates, increases with increasing mass. The increase in FRIM with increasing mass indicates the mass growth by aggregation plays a stronger role in the total mass when ice crystals are large and weigh more.

The increasing FRIM of plates and decreasing FRIM of dendrites can be explained by considering two crystals of equal diameter, a plate and a dendrite, falling through a cloud and collecting an equal mass. The mass collected will make up a greater fraction of the dendrites existing mass than plates causing the FRIM of dendrites to increase and plates to decrease with increasing mass (equations 23 and 24). Plates and dendrites have a different relationship between FRIM versus crystal mass. The FRIM by aggregation plays a greater role in the mass growth of dendrites compared to plates for snow aggregates that weigh more than 10^{-5} g.

6.2 *A comparison of the fractional rate of increase of mass by aggregation to the fractional rate of increase of mass by diffusion*

The data presented in Rogers and Yau (1989, p. 168) indicate the FRIM by diffusion, for a dendrite of mass 10^{-8} g to 10^{-4}g, decreases with increasing mass and lies within the range of 3×10^{-4} and 5×10^{-2} s^{-1}. This FRIM by diffusion can be used to determine the FRIM by diffusion for plates at -5°C by changing the diffusional variables, which vary with temperature, as given in Byers (1965, p. 120). In doing so, the resulting FRIM by diffusion for plates and dendrites can be compared (Figure 6.2). Both FRIM by diffusion decrease with increasing ice crystal mass, however, the slope of the FRIM of plates is steeper than that of dendrites. This shows that diffusion plays a

greater role in mass formation for small planar crystals compared to dendrites. But for large crystals dendrites grow by diffusion more than plates.

Comparing the FRIM by ice aggregation and deposition-diffusion shows that plates at -5°C grow predominantly by diffusion until they reach a mass of 2×10^{-7} g where the dominant method of growth changes to aggregation. Dendrites at -15°C also grow predominantly by diffusion when they are small; however, diffusion continues to be the dominant form of growth until the dendrites reach 2×10^{-6} g when aggregation becomes the predominant form of growth.

Table 6.1 Growth by aggregation vs. diffusion for plates and dendrites weighing 10^{-8} g to 10^{-3} g.

	Mass				
Ice Crystal Shape	**10^{-8} to 10^{-7} g**	**10^{-7} to 10^{-6} g**	**10^{-6} to 10^{-5} g**	**10^{-5} to 10^{-4} g**	**10^{-4} to 10^{-3} g**
Plate	Diffusion	Aggregation	Aggregation	Aggregation	Aggregation
Dendrite	Diffusion	Diffusion	Aggregation	Aggregation	Aggregation

6.3 Summary

The fractional rate of increase of mass (FRIM) by aggregation is dependent on temperature and type of ice crystal. Plates have a FRIM which decreases with increasing ice crystal mass, whereas dendrites have a FRIM which increases with increasing ice crystal mass. The decreasing FRIM of plates indicates that aggregation is important in the initial stages of growth. Dendrites, however, have a FRIM which increases with increasing mass, indicating that aggregation is more significant when ice crystals are larger. When comparing growth by aggregation versus deposition-diffusion, the estimates suggest that diffusion is dominant when snow aggregates are small. Specifically, the growth by deposition-diffusion exceeds that of aggregation for plates (at -5°C) at less than 10^{-7} g. For dendrites (at -15°C), the threshold is 10^{-6} g when aggregation starts to dominate deposition-diffusion.

7. CONCLUSIONS AND FUTURE WORK

7.1 *Conclusions*

Lin *et al.* (1983) and Cotton *et al.* (1986) developed a cloud-model ice parameterization scheme that included a bulk-water parameterization for ice aggregation. Both these studies assumed air temperature affected the collection efficiency of colliding ice crystals; however, they neglected to assume temperature affects the fall velocities of ice crystals, the fall velocities of snow aggregates, the mass-diameter relationship of crystals or aggregates, and the cross sectional areas of hydrometeors.

In this thesis we extend Cotton's aggregation parameterization scheme by including the effects of temperature on all parameters affecting growth by collection. Specifically, we assume that temperature determines the ice crystal shape. For temperatures colder than or equal to -12°C, it is assumed that the ice crystals are generally dendrites and that aggregates have properties resembling dendritic-shaped crystals. For temperatures warmer than or equal to -8°C, it is assumed that the ice crystals are generally plates and that aggregates resemble plate-shaped crystals. For temperatures between -12°C and -8°C, we assumed that there is a mixture of dendrites and plates. The relative concentration of dendrites versus plates is obtained by linear interpolation. Using these assumptions, we attain relationships between mass and size, cross-sectional area and size, and terminal fall velocity and size. The combination of these relationships yields a mass growth equation due to ice crystal aggregation which is based on model-resolved variables. Specifically we find a rate of aggregation in terms of snow aggregate mixing ratio (snow mixing ratio), ice crystal mixing ratio (cloud ice mixing ratio), temperature, and air density.

Our model equations indicate that for a fixed crystal mass, dendrites have a smaller fall velocity than plates. Thus an increase in temperature is associated with an increase in fall velocity of a snow aggregate. This affects the mass growth rate of a snow aggregate, and consequently the collection rate of ice crystals by snow aggregates. To investigate the impact of temperature (or ice crystal shape) on the collection rate of ice

crystals by snow aggregates, we first computed the "geometric collection rate", which is defined as the collection rate assuming a collection efficiency of 100%. One can think of the geometric collection rate as the collision rate of ice hydrometeors. The geometric collection rate is approximately proportional to the snow aggregate's fall velocity. As a result, the geometric collection rate at colder temperatures is less than that at warmer temperatures. One of the reasons for this is that plates have a faster fall velocity than dendrites of equal sizes. The fall velocity of dendrites is roughly half that of plates and as a result the geometric collection rate of dendrites is about half that of plates.

When comparing the (complete) collection rate of ice aggregation, the dependence on temperature is even more apparent. This is because the collection efficiency increases exponentially with increasing temperature. Consistent with previous studies, we find that the rate of ice aggregation ranges from approximately 10^{-7} to 10^{-5} $gg^{-1}s^{-1}$ depending on temperature. The increase in aggregation rate with increasing temperature indicates that the growth of the mixing ratio of snow aggregates (r_a) is very sensitive to the air temperature. The hundred-fold change in collection rate corresponds roughly to a hundred-fold increase of growth time.

We examine the effect of the snow aggregate size distribution on the ice aggregation rate. The chosen exponential size distribution, representing unmelted snow aggregates of all three shapes, is a function of a characteristic diameter. While the average characteristic diameter of Rogers' (1974) observations was 0.33 cm, characteristic diameters were found to range from 41 to 278% of this. In this thesis, the results from distributions with characteristic diameters equal to 50 to 250% of the control characteristic diameter 0.3 cm resulted in collection rates equal 20 to 866% of the control collection rate. Snow aggregate size distributions with larger characteristic diameters have a greater number of larger particles resulting in broader distributions. Broader distributions, in turn, have greater collection rates because there are a greater number of large snow aggregates with greater cross-sectional areas and therefore greater mass growth rates.

Using the equation for mass growth rate and the relationship of mass to size, the fractional rate of increase of mass can be determined. This rate quantifies the importance of the mass growth rate by aggregation, to the total mass of an aggregate. The fractional

rate of increase of mass by aggregation for plates differs significantly for that of dendrites in that plates have a fractional rate of increase of mass (FRIM) which decreases with increasing mass. In contrast, the fractional rate of increase of mass of dendrites increases with increasing mass. In other words, the temperature affects the slope of the FRIM-mass curve.

The fractional rate of increase of mass of plates and dendrites by aggregation can be compared to the fractional rate of increase of mass by diffusion of plates at -5°C and dendrites at -15°C. The comparison found plates greater than 10^{-7} g grows mainly by aggregation while plates less than 10^{-7}g grow mainly by diffusion. Similarly, dendrites greater than 2×10^{-6}g grow mainly by aggregation while dendrites less than 2×10^{-6} g grow mainly by diffusion. The fractional rate of increase of mass by diffusion of plates is greater than dendrites when snow aggregates are small. Diffusional growth, however, is a dominant form of growth for dendrites than plates. The fractional rate of increase of mass shows growth by aggregation is more significant to dendrites than plates when aggregates are greater than 10^{-5}g.

Our main conclusion is that temperature affects the aggregation process and thereby should be included in a bulk-water parameterization scheme of ice aggregation. The changes caused by ice crystal shape, in conjunction with the effects of collection efficiency, have significant effects on the mass growth rate and collection rate.

7.2 Future work

There are several components of our thesis research that would require further investigation. Possibly, the most important component of improving the bulk-water parameterization scheme of ice aggregation is to improve the quantification of the collection efficiency of interacting ice crystals. There are disturbing differences in some of the experimental studies that have tried to relate the collection efficiency to various ice crystal parameters. Most laboratory experiments suggest that warmer temperature increases the adhesion of colliding ice crystals, however, the exact relationship between temperature and collection efficiency requires additional work. Further investigation into whether the collection efficiency is dependent upon ice crystal shape would be of

interest, especially since it is mentioned but not quantified in previous research (Rogers and Yau, 1989 p.165, Khain and Sednev, 1996).

Secondly, there is a need to quantify the different broadness of size distributions for different ice crystal shapes. Ohtake (1970) reported that a snowflake size distribution of dendrites, with its fine branches, tended to aggregate to produce broad distributions (i.e. contains a greater number of large snow aggregates). In contrast, plates did not aggregate and produced narrower size distributions. More observations are essential either to support or refute Ohtake's (1970) findings.

Thirdly, the snowfall rate needs to be defined in terms of unmelted ice crystal diameter. By doing so, it would be possible to develop a relationship between the snowfall rate and characteristic diameter; which would allow the collection rate to be written in terms of snow aggregate mixing ratio (r_a) rather than the characteristic diameter (D_m) - as in Lin *et al.* (1983). Rogers (1974) states that broader distributions produce larger snow aggregate snowfall rates but his attempt to define the snowfall rate for wet and dry snowflakes in terms of the unmelted aggregate diameter was not successful.

Lastly, in the interest of determining the temperature ranges in which large aggregates are produced, a parameterization scheme that includes both ice crystal growths by diffusion and aggregation is necessary. When ice crystals are recently nucleated, they exist in an environment highly favorable for diffusional growth because the environment contains supercooled drops and is saturated relative to liquid water and supersaturated relative to ice. Consequently, ice crystals grow by diffusion of vapour at the expense of evaporating drops. The supercooled drops provide a continuous source of moisture for the growing ice crystals until there are no more supercooled drops available for evaporation and the vapor pressure equilibrium relative to water can no longer be maintained. The rate of diffusional growth reaches a maximum at approximately -15°C (Byers, 1965, p.123). An ice crystal grows to tens of microns by diffusional growth in a few minutes. Combining this knowledge with the results of the collection rate by aggregation, which is greatest near 0°C and decreases with decreasing temperature, would possibly result in two zones of large aggregate formation. The first is near 0°C where maximum adhesion between ice crystals occurs and the second is near -12 to -

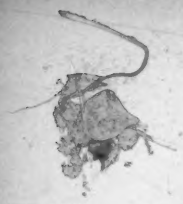

15°C where aggregation between a few, yet large, ice crystals can create large aggregates. These results would corroborate the findings of Hobbs *et al.* (1974) and Yeh *et al.* (1986).

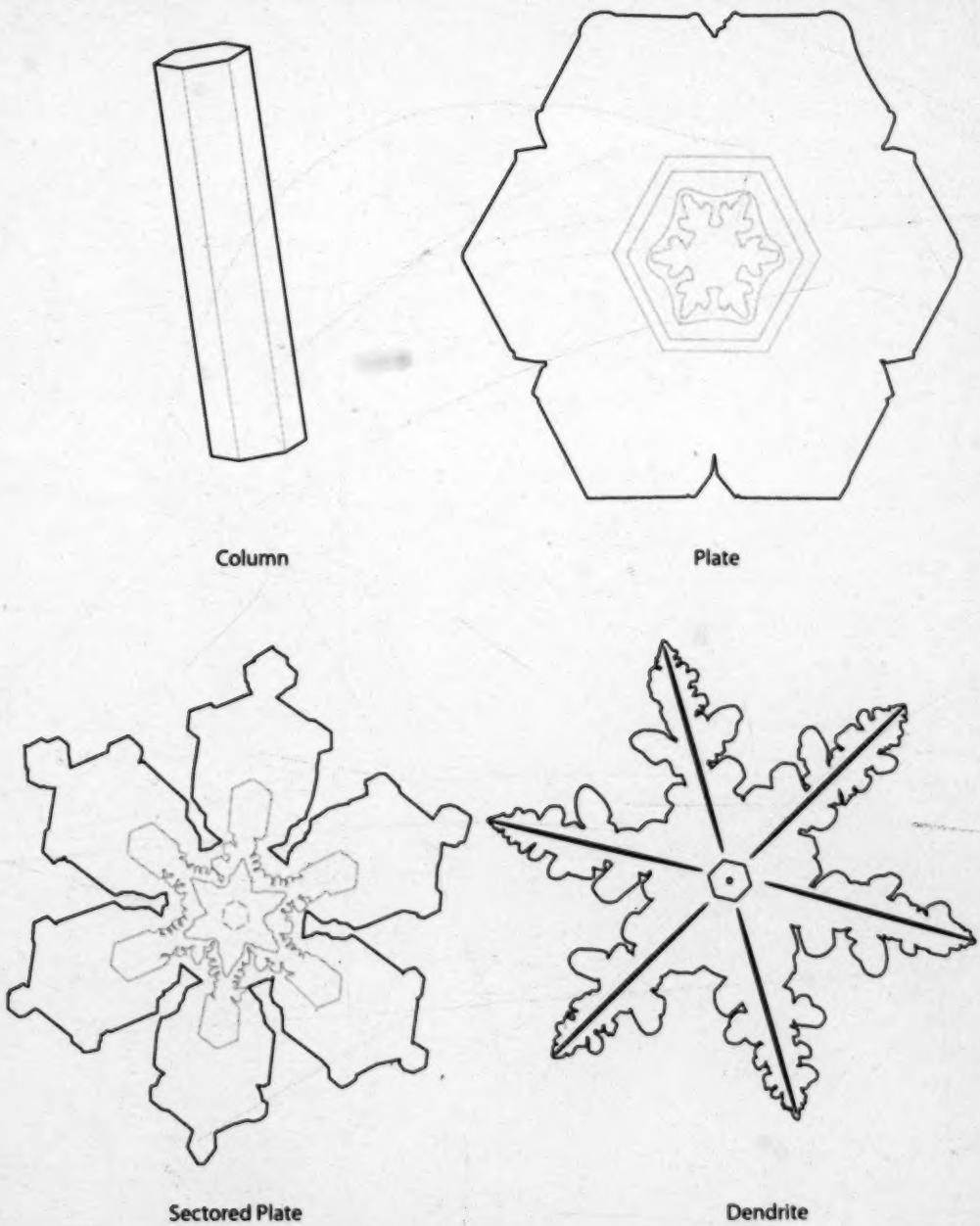

Figure 1.1 A schematic representation of typical ice crystal shapes.

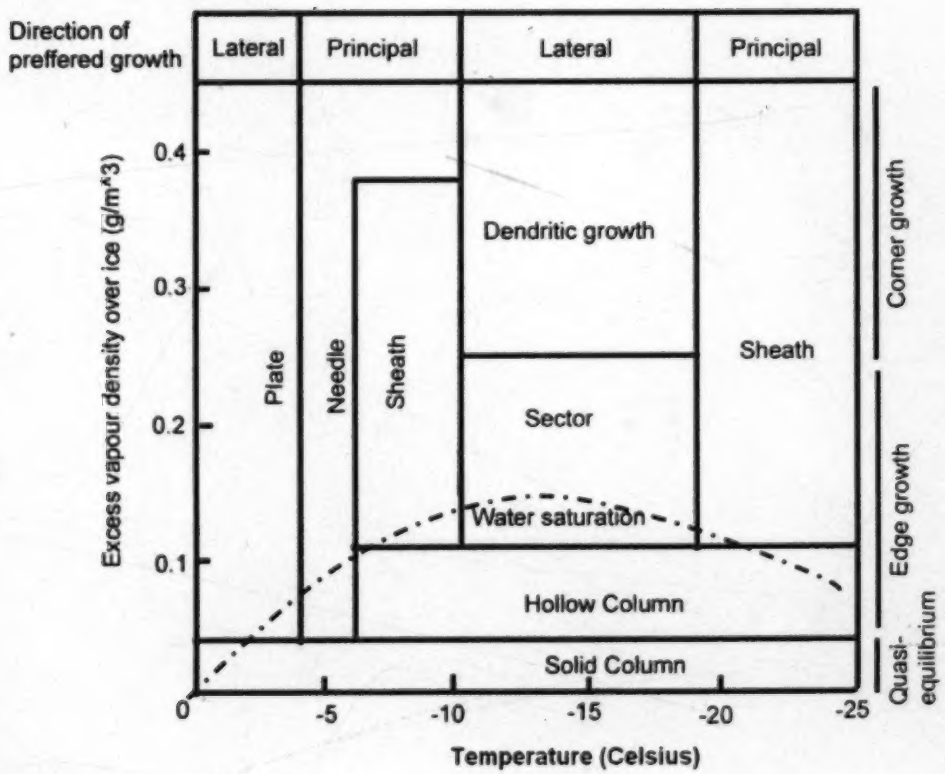

Figure 1.2 An ice crystal classification scheme as a function of temperature (°C) and excess vapour density over ice saturation (g m^{-3}) adopted from Kobayashi's (1958).

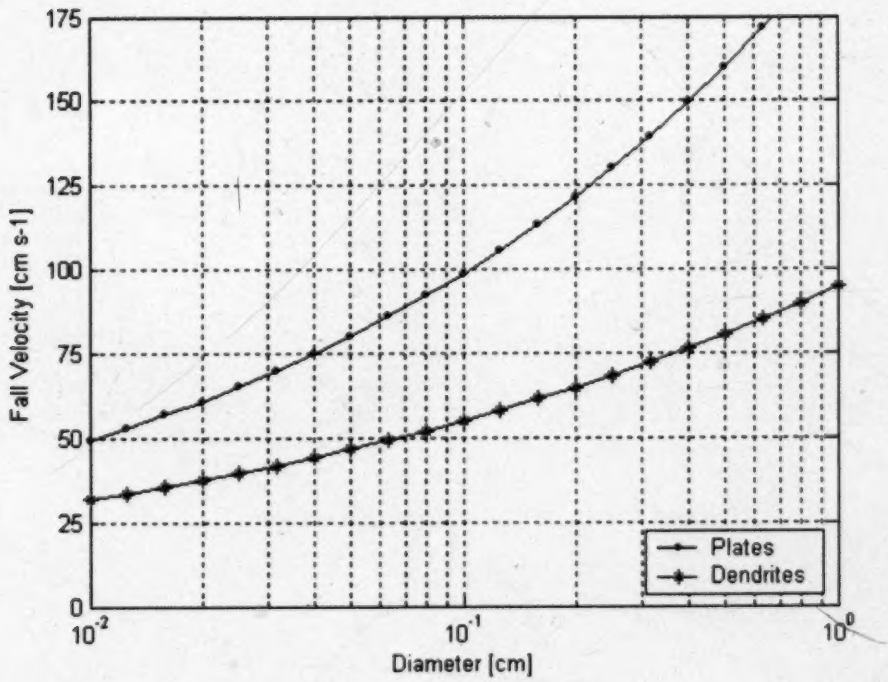

Figure 2.1 The fall velocity (cm s^{-1}) of plate and dendrites snow aggregates as a function of unmelted diameter (cm).

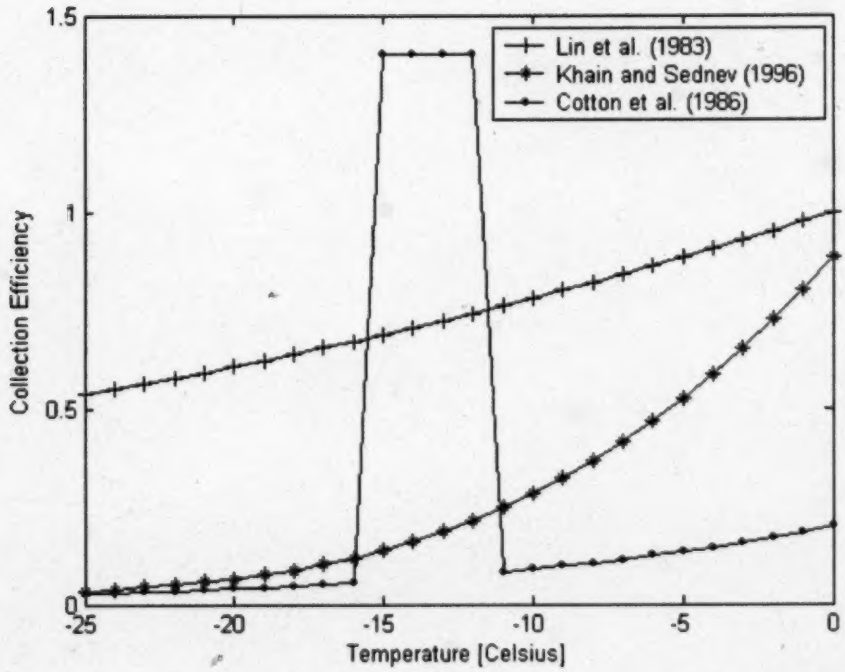

Figure 2.2 A comparison of the collection efficiencies (E) of Lin *et al.* (1983), Cotton *et al.* (1986), and Khain and Sednev (1996).

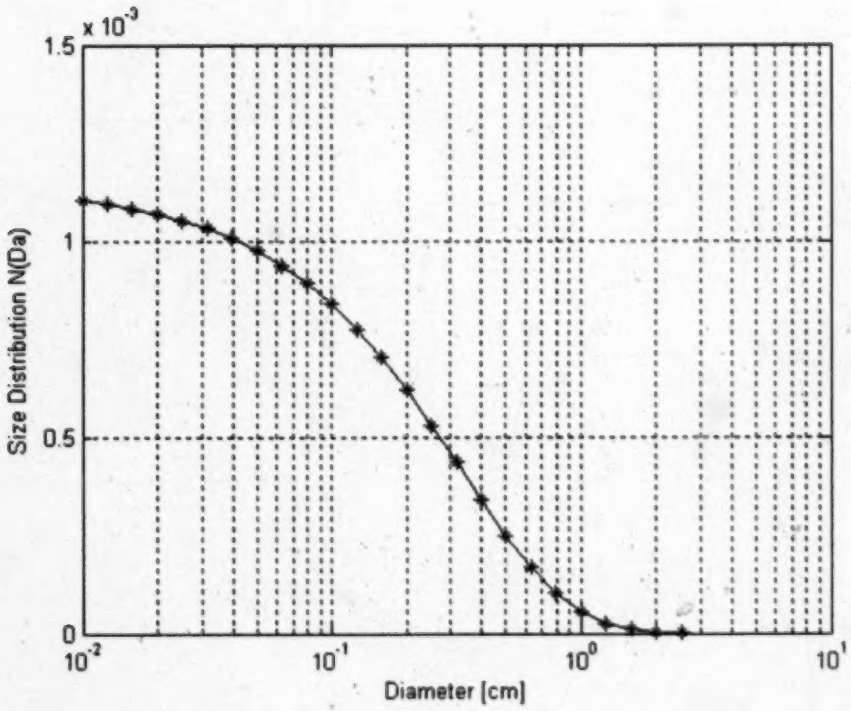

Figure 3.1 A typical inverse exponential snow aggregate size distribution $N(D_a)$.

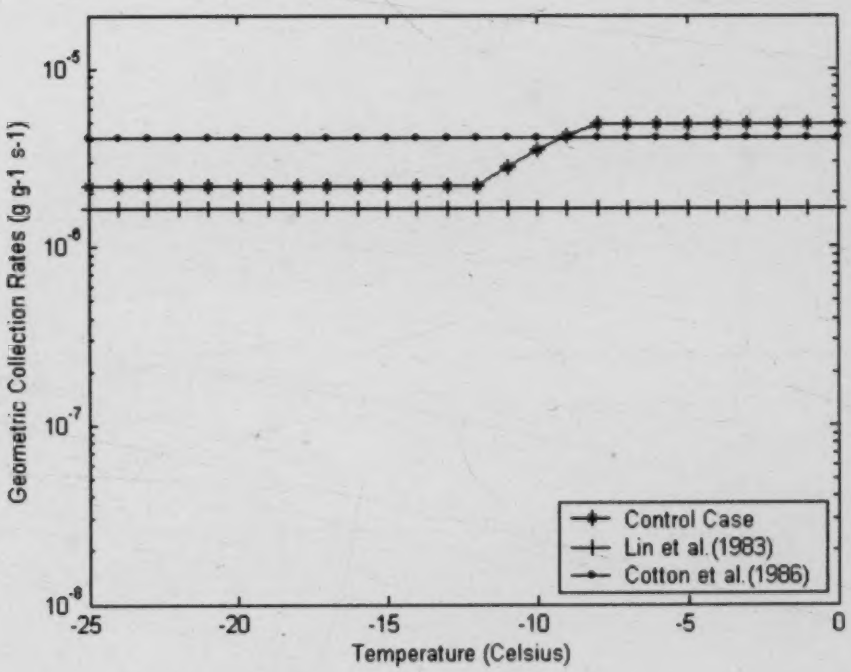

Figure 4.1 The geometric collection rates ($g\ g^{-1}\ s^{-1}$) of the control case, Lin *et al.* (1983), and Cotton *et al.* (1986) versus temperature (°C).

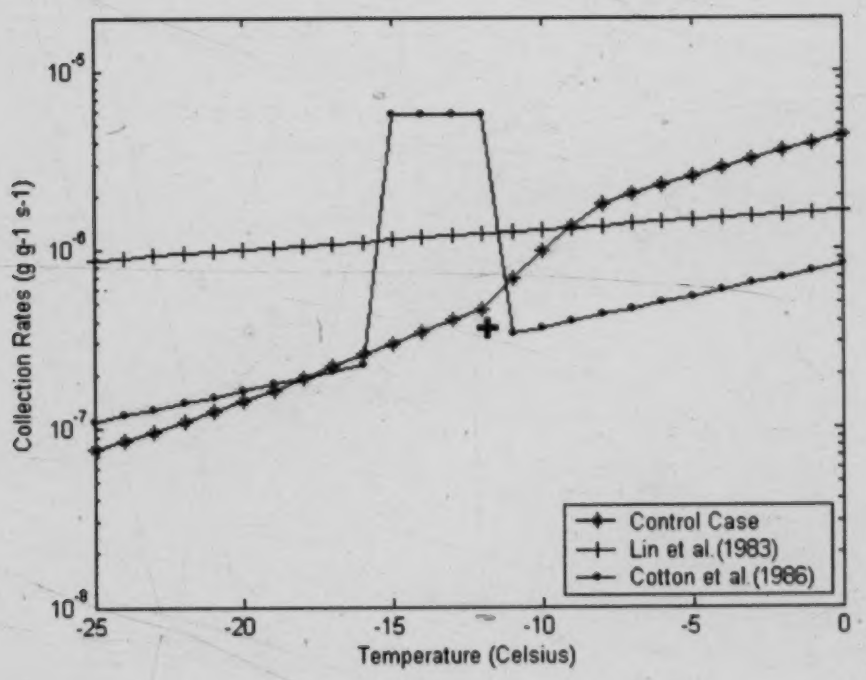

Figure 4.2 The collection rates (g g^{-1} s^{-1}) of the control case, Lin *et al.* (1983), and Cotton *et al.* (1986) versus temperature (°C). The collection rate of Khain and Sednev (1995) at -12°C, is denoted by ✚.

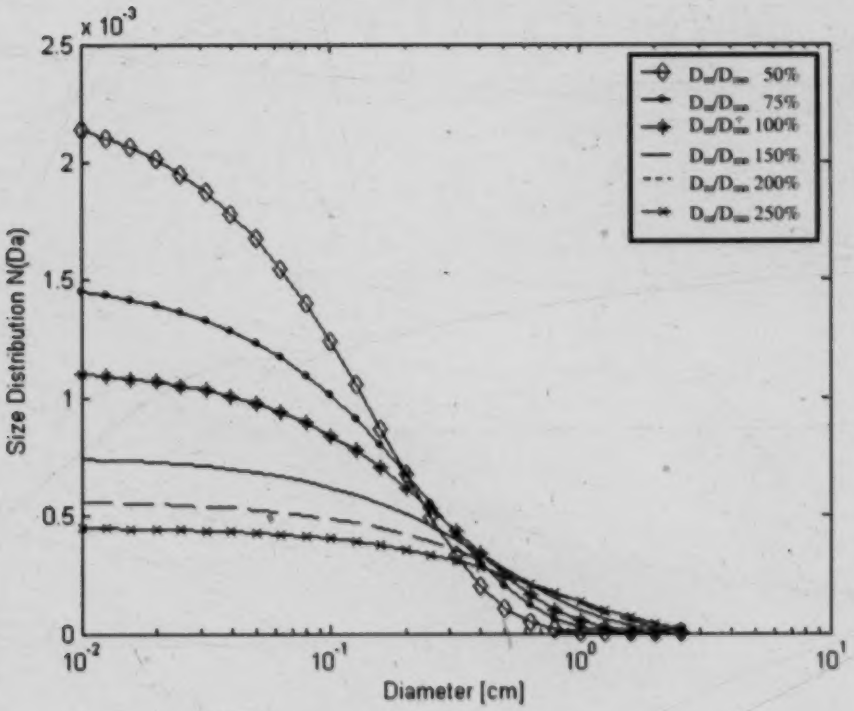

Figure 5.1 The snow aggregate size distributions (cm^{-4}) with characteristic diameters equal 50, 75, 100, 150, 200, and 250% of the control case characteristic diameter (D_{mo} = 0.33 cm).

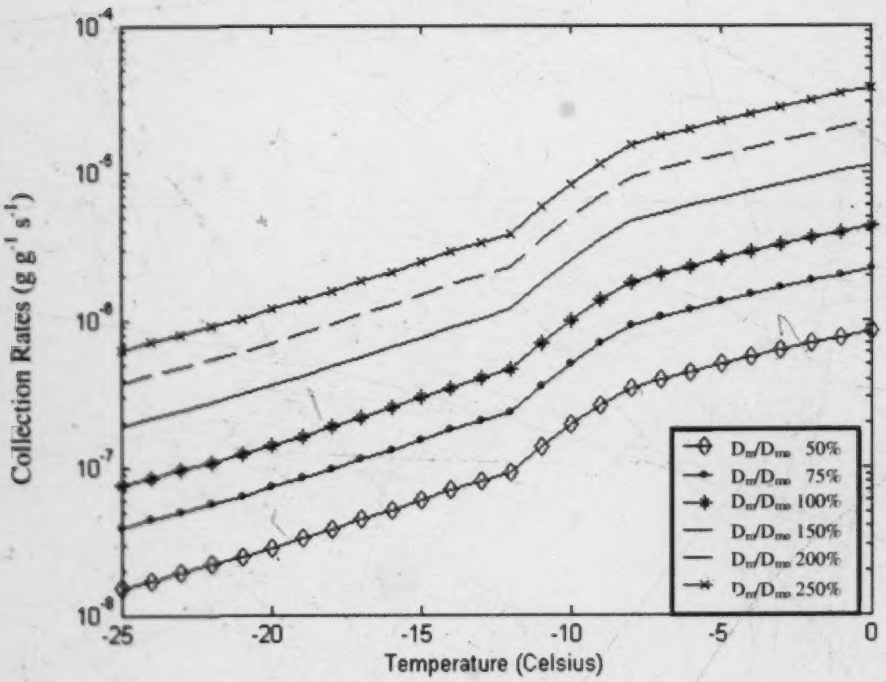

Figure 5.2 The collection rates (g g^{-1} s^{-1}) with snow aggregates size distributions with characteristic diameters equal to 50, 75, 100, 150, 200, and 250% of the control case characteristic diameter (D_{mo} = 0.33 cm).

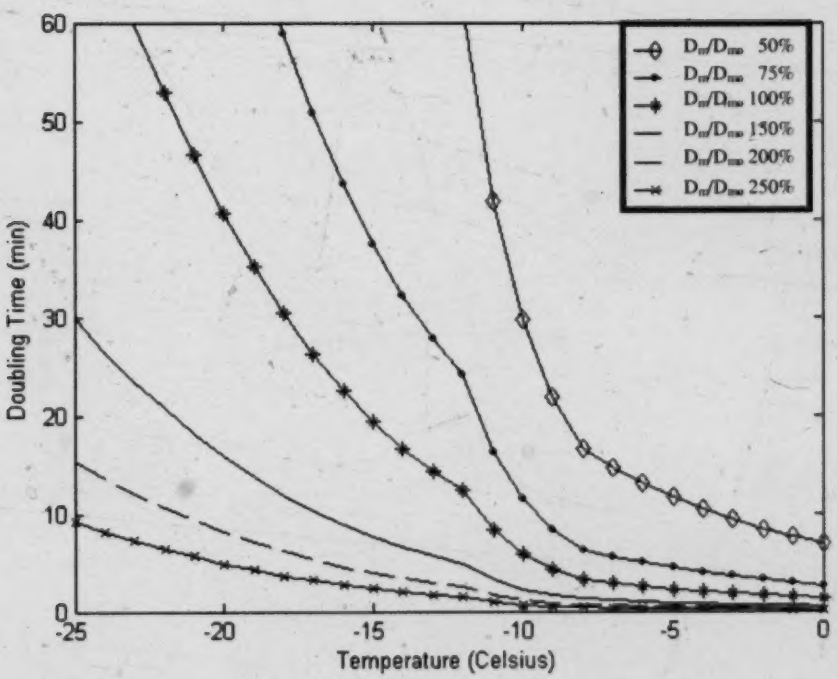

Figure 5.3 The time (min) required for the mixing ratio of snow aggregates to double for collection rates with size distributions using characteristic diameters equal to 50, 75, 100, 150, 200, and 250% of the control case characteristic diameter (D_{mo} = 0.33 cm).

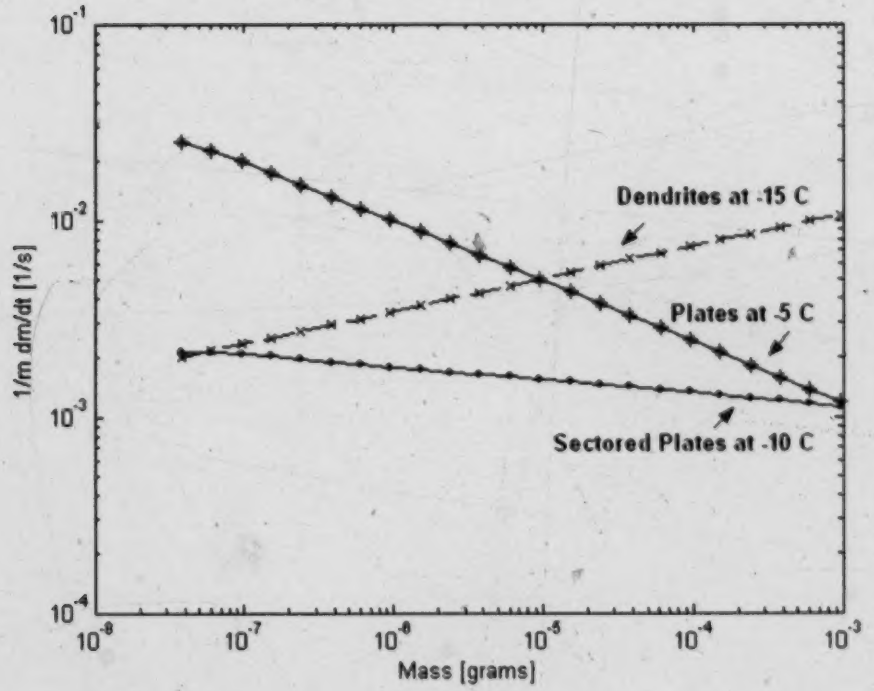

Figure 6.1 The fractional rate of increase of mass (s^{-1}) by aggregation of plates at -5°C, sector plates at -10°C, and dendrites at -15°C.

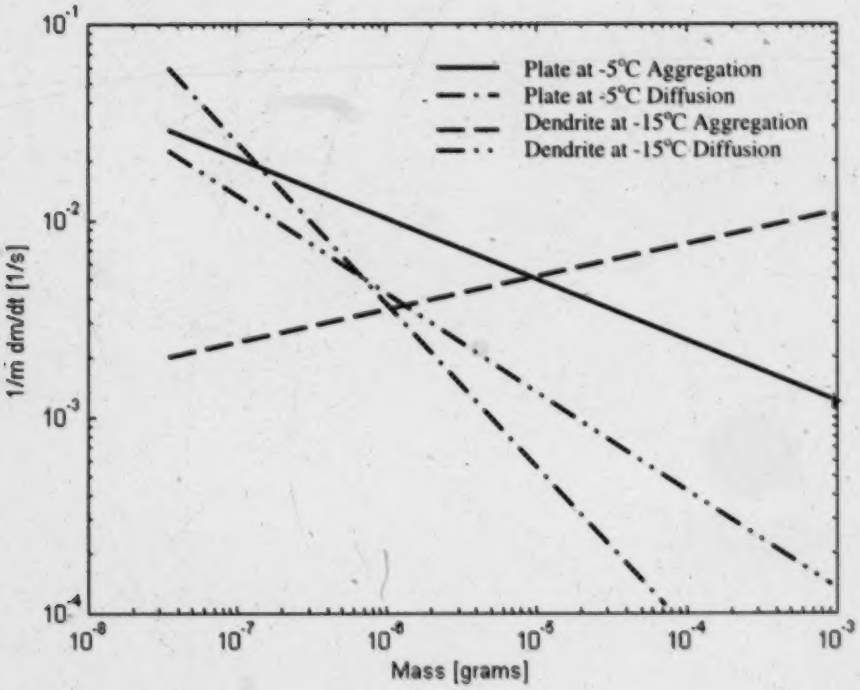

Figure 6.2 The fractional rate of increase of mass (s^{-1}) by aggregation and diffusion of plates at -5°C and dendrites at -15°C.

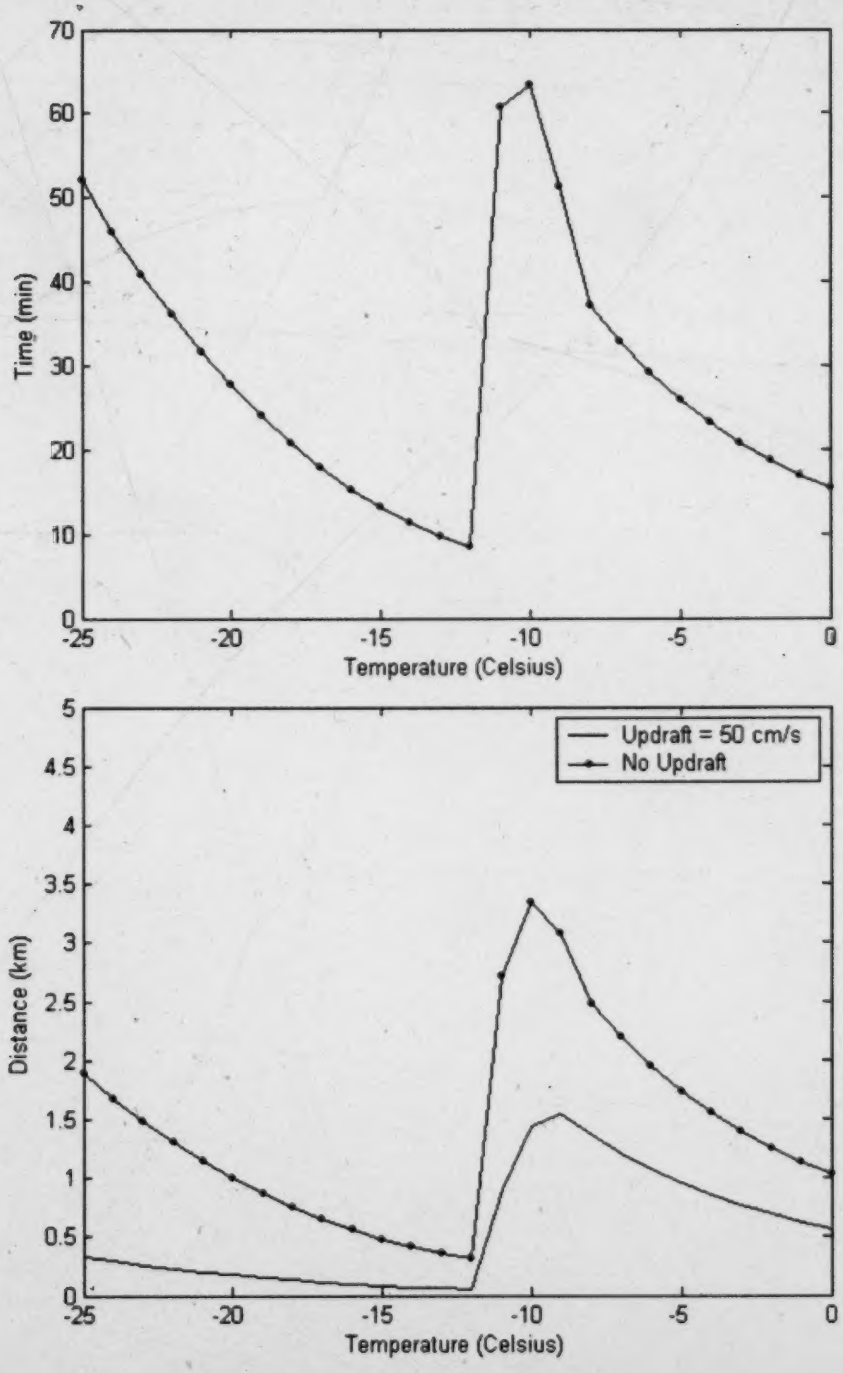

Figure 7.1 The maximum time (minute) and maximum distance (km) required for a snow aggregate's diameter to grow from 0.005 to 0.15 cm versus temperature (°C).

REFERENCES

Auer, Jr., A.H., 1971a: Some large snowflakes. *Weather*, **26**, 121-122.

Böhm, J.P., 1992: A general hydrodynamic theory for mixed-phase microphysics. Part III: Riming and aggregation. *Atmos. Re.*, **28**, 103-123.

Byers, H.R. Elements of Cloud Physics. University of Chicago Press, 1965.

Cotton, W.R. and R.A. Anthes. Storm and Cloud Dynamics. Academic Press, Inc., 1989.

Cotton, W.R., G.J. Tripoli, R.M. Rauber, and E.A. Mulvihill, 1986: Numerical simulation of the effects of varying ice crystal nucleation rates and aggregation processes on orthographic snowfall. *J. Atmos. Sci.*, **25**, 1658-1680.

Diamond, M. and W.P. Lowry, 1954: Correlation of density of new snow with 700-millibar temperature. *J. Atmos. Sci.*, **11**, 512-513.

Dupilka, M., and G.W. Reuter, 2004: On predicting maximum snowfall amounts in Alberta. *Atmos.Ocean*, (accepted with revisions).

Gunn, K.L.S. and J.S. Marshall, 1958: The distribution with size of aggregate snowflakes. *J. Meteor.*, **15**, 452-461.

Hall, W.D., 1980: A detailed microphysical model within a two-dimensional dynamic framework: Model description and preliminary results. *J. Atmos. Sci.*, **37**, 2486-2507.

Hallett, J., 1984: How snow crystals grow. *Am. Sci.*, **72**, 582-589.

Hallgren, R.E. and C.L. Hosler, 1960: Preliminary results on the aggregation of ice crystals. *Geophys. Monogr., Am. Geophys. Union*, No. **5**,257-263.

Hobbs, P.V. *et al.*, 1972. Contributions from the cloud physics group. Res. Rep. VII, Dept. of Atmos. Sci., Univ. of Wash., Seattle, 293 p.

Hobbs, P.V., S. Chang, and J. Locatelli, 1974: The dimensions and aggregation of ice crystals in natural clouds. *J. Geophys. Res.*, **79**, 2199-2206.

Hosler, C.L., Capt. D.C. Jensen, USAF and Pvt. L. Goldshlak, USA, 1957: On the aggregation of ice crystals to form snow. *J. Meteorology*, **14**, 415-420.

Hosler, C.L. and R.E. Hallgren, 1960: The aggregation of small ice crystals. *Discuss. Faraday Soc.*, **30**, 200-208.

Houghton, H.G. Physical Meteorology. MIT Press, Cambridge University, Mass., 442 p.

Khain, A.P. and I.L. Sednev, 1995: Simulation of hydrometeor size spectra evolution by water-water, ice-water and ice-ice interactions. *Atmos. Res.*, **36**, 107-138.

Khain, A.P. and I.L. Sednev, 1996: Simulation of precipitation in the Eastern Mediterranean costal zone using a spectral microphysics cloud ensemble model. *Atmos. Res.*, **43**, 77-110.

Kobayashi, T., 1958: On the habit of snow crystals artificially produced at low pressures. *J. Met. Soc. Japan*, Series 2, **36**, 193.

Latham, J. and C.P.R Sunders, 1971: Experimental measurements of the collection efficiencies of ice crystals in electric fields. *Quart. J. Roy. Meteor. Soc.*, **96**, 257-265.

Langleben, M.P., 1954: The terminal velocity of snowflakes. *Quart. J. Roy. Meteor. Soc.*,**80**: 174-181.

Lin, Y.L., R.D. Farley, and H.D. Orville, 1983: Bulk parameterization of the snow field in a cloud model. *J. Climate Appl. Meterol.*, **22**, 1065-1092.

Locatelli, J.D. and P.V. Hobbs, 1974: Fall speeds and masses of solid precipitation particles. *J. Geophys. Reseach*, **79**, 2185-2197.

Magano, C., 1953: On the growth of snowflake and graupel. *Science Report, Yokohama National University*, Section I, No. 2, 18-40.

Magano, C., 1960: Structure of snowfall revealed by geographic distribution of snow crystals. *Physics of Precipitation*, Geophysical Monograph No. 5, American Geophysical Union, Washington, D.C., 142-161.

Ohtake, T., 1970: Factors affecting the size distributions of hydrometeors through the melting layer. *J. Atmos. Sci.*, **27**, 804-813.

Passarelli, R.E, 1978: Theoretical and observational study of snow-size spectra and snowflake aggregation efficiencies. *J. Atmos. Sci.*, **35**, 882-889.

Power, B.A., 1962: Relationship between density and newly fallen snow and form of snow crystals. *Nature*, **193**, 1171.

Reuter, G. W., and R. Beaubien, 1996: Radar observations of snow formation in a warm pre-frontal snowband. *Atmos.-Ocean*, **34**, 605-626.

Rogers, D.C., 1974: The aggregation of natural ice crystals. M.S. thesis, Dept. of Atmospheric Resources, University of Wyoming.

Rogers, R.R. and M.K. Yau. A Short Course in Cloud Physics, 3rd Edition. Pergamon Press, 1989.

Sasyo, Y., 1971: Study of the formation of precipitation by the aggregation of snow particles and the accretion of cloud droplets on snowflakes. *Pap. Meteor. Geophys.*, **22**, 69-142.

Yeh, J., M. Fortune and W. Cotton, 1986: Microphysics of the stratified precipitation region of a mesoscale convective system. Prep., *Conf. Cloud Phys., Snowmass, Colo.* pp. J151-J154. Am. Meteorol. Soc., Boston, Massachusetts.

Appendix A: List of Symbols

	Notation	Value	Units
Subscript i denotes ice crystals	i		
Subscript a denotes snow aggregates	a		
Characteristic diameter	D_m		cm
Control characteristic diameter	D_{mo}	0.33	cm
Collection efficiency	E		
Collection rate	C		$g\ g^{-1}\ s^{-1}$
Cross sectional area	A		cm^2
Density of air (at 3 km)	ρ	0.000909	$g\ cm^{-3}$
Density at surface	ρ_o	0.001225	$g\ cm^{-3}$
Density of ice	ρ_a	0.1	$g\ cm^{-3}$
Diameter of ice crystals	D_i	0.005	cm
Diameter of snow aggregates	D_a		cm
Equivalent diameter of water drop when ice crystals and snow aggregates are melted	$D_{equivalent}$		cm
Fall velocity of ice crystals and snow aggregates	V		$cm\ s^{-1}$
Fall velocity parameter	c	169.7	For plates
		81.9	For dendrite
	d	0.3	For plates
		0.237	For dendrite
Fall velocity inertial response	δV	2	$cm\ s^{-1}$
Mass of ice crystals and snow aggregates	M		g
Mass parameter	a	0.019	For plates
		0.00038	For dendrite
	b	3	For plates
		2	For dendrite
Mixing ratio of ice crystals	r_i	0.0005	$g\ g^{-1}$
Mixing ratio of snow aggregates	r_a	0.0005	$g\ g^{-1}$
Relative humidity	RH		
Snow aggregate size distribution	$N(D_a)$		cm^{-4}
Snow aggregate size distribution intercept parameter	N_o		cm^{-4}
Snow aggregate size distribution slope parameter	λ_a		cm^{-1}
Temperature	T		°C

Appendix B: Fall Velocity

The terminal fall velocities of an individual ice crystal V_i and a snow aggregate V_a (in cm s^{-1}) are given by

$$V_i = c(D_{equivalent})^d \left(\frac{\rho_o}{\rho}\right)^{1/2},$$

$$V_a = c(D_{equivalent})^d \left(\frac{\rho_o}{\rho}\right)^{1/2},$$

where $D_{equivalent}$ is the diameter of the liquid drop when the snow aggregate is melted (cm) and ρ is air density (g cm^{-3}), and ρ_o is surface air density (g cm^{-3}). The square root of air densities accounts for the increasing fall velocity with increasing altitude (Lin *et al.*, 1983). Based on Langleben (1954) the values for c and d are $c \approx 234$ and $d \approx 0.3$ for plates and for dendrites $c \approx 160$ and $d \approx 0.3$ for dendrites. We need to express $D_{equivalent}$ in terms of the ice crystal/snow aggregate diameter (major linear dimension). From Mason (1971) and Houghton (1985) the mass of an ice crystal, in terms of the crystal diameter, is given as

$$M_i = aD_i^b,$$

$$M_a = aD_a^b,$$

where M_i and M_a are in g, and D_i and D_a are in cm. For plates $a = 0.019$ and $b=3$; and for dendrites, $a= 0.00038$ and $b = 2$. Khain and Sednev (1995) state the densities of plates are 0.9 g cm^{-3} whereas dendrites are equal 0.588 x $(D_{i,a})^{-0.377}$. Thus for plates:

$$Mass = Volume \times Density$$

$$0.019(D_{i,a})^3 = \frac{4\pi}{3}\left(\frac{D_{equivalent}}{2}\right)^3 \times 0.9$$

$$\frac{3\times 0.019}{4\pi \times 0.9}(D_{i,a})^3 = \left(\frac{D_{equivalent}}{2}\right)^3$$

$$(0.00504)^{1/3} D_{i,a} = \frac{D_{equivalent}}{2}$$

$$0.343 D_{i,a} = D_{equivalent}$$

$$Fall\ Velocity = c\,(D_{equivalent})^d$$

$$V_{i,a} = 234\,(0.343\,D_{i,a})^{0.3}$$

$$V_{i,a} = 169.7\ (D_{i,a})^{0.3}$$

And for dendrites:

$$Mass = Volume \times Density$$

$$0.00038(D_{i,a})^2 = \frac{4\pi}{3}\left(\frac{D_{equivalent}}{2}\right)^3 \times 0.588\left(D_{i,a}\right)^{-0.377}$$

$$\frac{3\times 0.00038}{4\pi\times 0.588}(D_{i,a})^{2.377} = \left(\frac{D_{equivalent}}{2}\right)^3$$

$$(0.00015428)^{1/3}\ (D_{i,a})^{0.7923} = \frac{D_{equivalent}}{2}$$

$$0.10727\ (D_{i,a})^{0.7923} = D_{equivalent}$$

$$Fall\ Velocity = c\ (D_{equivalent})^d$$

$$V_{i,a} = 160\left(0.10727\ (D_{i,a})^{0.7923}\right)^{0.3}$$

$$V_{i,a} = 81.9\ (D_{i,a})^{0.237}$$

Appendix C: Collection Rate (Ice Aggregation Rate)

$$C = \int_0^\infty \frac{1}{\rho}\frac{dM}{dt}\, N(D_a)\, dD_a$$

$$C = \int_0^\infty A\, (|V_a - V_i| + \delta V)\; r_i\, E\, N_o \exp(-\lambda_a D_a)\, dD_a$$

$$C = \int_0^\infty \frac{\pi}{4}(D_a + D_i)^2 \left(\left| cD_a{}^d \left(\frac{\rho_o}{\rho}\right)^{0.5} - cD_i{}^d \left(\frac{\rho_o}{\rho}\right)^{0.5} \right| + \delta V \right) r_i\, E\, N_o \exp(-\lambda_a D_a)\, dD_a$$

$$C = \frac{\pi}{4} E\, r_i\, N_o \int_0^\infty \left(D_a{}^2 + 2D_a D_i + D_i{}^2\right) \left(\left| cD_a{}^d \left(\frac{\rho_o}{\rho}\right)^{0.5} - cD_i{}^d \left(\frac{\rho_o}{\rho}\right)^{0.5} \right| + \delta V \right) \exp(-\lambda_a D_a)\, dD_a$$

$$C = \frac{\pi}{4} E\, r_i\, N_o \int_0^\infty \begin{bmatrix} \left(cD_a{}^{2+d}\left(\frac{\rho_o}{\rho}\right)^{0.5}\right) - \left(cD_a{}^2 D_i{}^d \left(\frac{\rho_o}{\rho}\right)^{0.5}\right) + \left(\delta V\, D_a{}^2\right) \\ + \left(2c\, D_a{}^{1+d} D_i \left(\frac{\rho_o}{\rho}\right)^{0.5}\right) - \left(2c\, D_a D_i{}^{1+d}\left(\frac{\rho_o}{\rho}\right)^{0.5}\right) + \left(2\delta V\, D_a D_i\right) \\ + \left(cD_a{}^d D_i{}^2 \left(\frac{\rho_o}{\rho}\right)^{0.5}\right) - \left(cD_i{}^{2+d}\left(\frac{\rho_o}{\rho}\right)^{0.5}\right) + \left(\delta V\, D_i{}^2\right) \end{bmatrix} \exp(-\lambda_a D_a)\, dD_a$$

$$C = \frac{\pi}{4} E\, r_i\, N_o \int_0^\infty \begin{bmatrix} \left(c\left(\frac{\rho_o}{\rho}\right)^{0.5}\right) D_a{}^{2+d} + \left(\delta V - cD_i{}^d \left(\frac{\rho_o}{\rho}\right)^{0.5}\right) D_a{}^2 + \\ + \left(2c\, D_i \left(\frac{\rho_o}{\rho}\right)^{0.5}\right) D_a{}^{1+d} + \left(2\delta V\, D_i - 2c\, D_i{}^{1+d}\left(\frac{\rho_o}{\rho}\right)^{0.5}\right) D_a \\ + \left(c\, D_i{}^2 \left(\frac{\rho_o}{\rho}\right)^{0.5}\right) D_a{}^d + \left(\delta V\, D_i{}^2 - cD_i{}^{2+d}\left(\frac{\rho_o}{\rho}\right)^{0.5}\right) \end{bmatrix} \exp(-\lambda_a D_a)\, dD_a$$

$$C = \frac{\pi}{4} E\, r_i\, N_o \begin{bmatrix} \left(c\left(\frac{\rho_o}{\rho}\right)^{0.5}\right) \Gamma(3+d)\, \lambda_a{}^{-(3+d)} + \left(2cD_i \left(\frac{\rho_o}{\rho}\right)^{0.5}\right) \Gamma(2+d) \lambda_a{}^{-(2+d)} \\ + \left(cD_i{}^2 \left(\frac{\rho_o}{\rho}\right)^{0.5}\right) \Gamma(1+d) \lambda_a{}^{-(1+d)} + \left(\delta V - cD_i{}^d \left(\frac{\rho_o}{\rho}\right)^{0.5}\right) \Gamma(3)\, \lambda_a{}^{-3} \\ + \left(2\delta V\, D_i - 2cD_i{}^{1+d}\left(\frac{\rho_o}{\rho}\right)^{0.5}\right) \Gamma(2) \lambda_a{}^{-2} + \left(\delta V\, D_i{}^2 - cD_i{}^{2+d}\left(\frac{\rho_o}{\rho}\right)^{0.5}\right) \Gamma(1) \lambda_a{}^{-1} \end{bmatrix}$$

Appendix D: Doubling Time (τ)

$$\frac{d\,r_a}{dt} = Collection\ Rate\,(C)$$

$$d\,r_a = Collection\ Rate\,(C) \times dt$$

$$d\,r_a = \frac{\pi}{4} E\, r_i\, N_o \left[\begin{array}{l} c\left(\frac{\rho_o}{\rho}\right)^{0.5} \Gamma(3+d)\,\lambda_a^{-(3+d)} + 2cD_i\left(\frac{\rho_o}{\rho}\right)^{0.5} \Gamma(2+d)\lambda_a^{-(2+d)} \\ + cD_i^{\,2}\left(\frac{\rho_o}{\rho}\right)^{0.5} \Gamma(1+d)\lambda_a^{-(1+d)} + \left(\delta V - cD_i^{\,d}\left(\frac{\rho_o}{\rho}\right)^{0.5}\right)\Gamma(3)\,\lambda_a^{-3} \\ + \left(2\delta V\, D_i - 2cD_i^{\,1+d}\left(\frac{\rho_o}{\rho}\right)^{0.5}\right)\Gamma(2)\lambda_a^{-2} + \left(\delta V\, D_i^{\,2} - cD_i^{\,2+d}\left(\frac{\rho_o}{\rho}\right)^{0.5}\right)\Gamma(1)\lambda_a^{-1} \end{array} \right] \times dt$$

$$d\,r_a = \frac{\pi}{4} E\, r_i\, N_{oo} \rho\, r_a\, D_m^{\,3} \left[\begin{array}{l} c\left(\frac{\rho_o}{\rho}\right)^{0.5} \Gamma(3+d)\,D_m^{\,(3+d)} + 2cD_i\left(\frac{\rho_o}{\rho}\right)^{0.5} \Gamma(2+d)D_m^{\,(2+d)} \\ + cD_i^{\,2}\left(\frac{\rho_o}{\rho}\right)^{0.5} \Gamma(1+d)D_m^{\,(1+d)} + \left(\delta V - cD_i^{\,d}\left(\frac{\rho_o}{\rho}\right)^{0.5}\right)\Gamma(3)\,D_m^{\,3} \\ + \left(2\delta V\, D_i - 2cD_i^{\,1+d}\left(\frac{\rho_o}{\rho}\right)^{0.5}\right)\Gamma(2)D_m^{\,2} + \left(\delta V\, D_i^{\,2} - cD_i^{\,2+d}\left(\frac{\rho_o}{\rho}\right)^{0.5}\right)\Gamma(1)D_m^{\,1} \end{array} \right] \times dt$$

$$\int \frac{1}{r_a} d\,r_a = \int \frac{\pi}{4} E\, r_i\, N_{oo} \rho D_m^{\,3} \left[\begin{array}{l} c\left(\frac{\rho_o}{\rho}\right)^{0.5} \Gamma(3+d)\,D_m^{\,(3+d)} + 2cD_i\left(\frac{\rho_o}{\rho}\right)^{0.5} \Gamma(2+d)D_m^{\,(2+d)} \\ + cD_i^{\,2}\left(\frac{\rho_o}{\rho}\right)^{0.5} \Gamma(1+d)D_m^{\,(1+d)} + \left(\delta V - cD_i^{\,d}\left(\frac{\rho_o}{\rho}\right)^{0.5}\right)\Gamma(3)\,D_m^{\,3} \\ + \left(2\delta V\, D_i - 2cD_i^{\,1+d}\left(\frac{\rho_o}{\rho}\right)^{0.5}\right)\Gamma(2)D_m^{\,2} + \left(\delta V\, D_i^{\,2} - cD_i^{\,2+d}\left(\frac{\rho_o}{\rho}\right)^{0.5}\right)\Gamma(1)D_m^{\,1} \end{array} \right] \times dt$$

$$\ln r_{a\,final} - \ln r_{a\,initial} =$$

$$\frac{\pi}{4} E\, r_i\, N_{oo} \rho D_m^{\,3} \left[\begin{array}{l} c\left(\frac{\rho_o}{\rho}\right)^{0.5} \Gamma(3+d)\,D_m^{\,(3+d)} + 2cD_i\left(\frac{\rho_o}{\rho}\right)^{0.5} \Gamma(2+d)D_m^{\,(2+d)} \\ + cD_i^{\,2}\left(\frac{\rho_o}{\rho}\right)^{0.5} \Gamma(1+d)D_m^{\,(1+d)} + \left(\delta V - cD_i^{\,d}\left(\frac{\rho_o}{\rho}\right)^{0.5}\right)\Gamma(3)\,D_m^{\,3} \\ + \left(2\delta V\, D_i - 2cD_i^{\,1+d}\left(\frac{\rho_o}{\rho}\right)^{0.5}\right)\Gamma(2)D_m^{\,2} + \left(\delta V\, D_i^{\,2} - cD_i^{\,2+d}\left(\frac{\rho_o}{\rho}\right)^{0.5}\right)\Gamma(1)D_m^{\,1} \end{array} \right] \times \left(t_{final} - t_{initial}\right)$$

Let $r_{a\ final}$ equal (2 x $r_{a\ initial}$) and τ denote ($t_{final} - t_{initial}$)

$$\ln\left(\frac{r_{a\ final}}{r_{a\ initial}}\right) =$$

$$\frac{\pi}{4} E\, r_i\, N_{\infty}\, \rho\, D_m^{-3.4} \left[\begin{array}{l} c\left(\frac{\rho_o}{\rho}\right)^{0.5} \Gamma(3+d) D_m^{(3+d)} + 2cD_i\left(\frac{\rho_o}{\rho}\right)^{0.5} \Gamma(2+d) D_m^{(2+d)} \\ + cD_i^2\left(\frac{\rho_o}{\rho}\right)^{0.5} \Gamma(1+d) D_m^{(1+d)} + \left(\delta V - cD_i^d\left(\frac{\rho_o}{\rho}\right)^{0.5}\right) \Gamma(3) D_m^3 \\ + \left(2\delta V\, D_i - 2cD_i^{1+d}\left(\frac{\rho_o}{\rho}\right)^{0.5}\right) \Gamma(2) D_m^2 + \left(\delta V\, D_i^2 - cD_i^{2+d}\left(\frac{\rho_o}{\rho}\right)^{0.5}\right) \Gamma(1) D_m^1 \end{array} \right] \times \tau$$

$$\tau = \frac{\ln\left(\frac{r_{a\ final}}{r_{a\ initial}}\right)}{\frac{\pi}{4} E\, r_i\, N_{\infty}\, \rho\, D_m^{-3.4} \left[\begin{array}{l} c\left(\frac{\rho_o}{\rho}\right)^{0.5} \Gamma(3+d) D_m^{(3+d)} + 2cD_i\left(\frac{\rho_o}{\rho}\right)^{0.5} \Gamma(2+d) D_m^{(2+d)} \\ + cD_i^2\left(\frac{\rho_o}{\rho}\right)^{0.5} \Gamma(1+d) D_m^{(1+d)} + \left(\delta V - cD_i^d\left(\frac{\rho_o}{\rho}\right)^{0.5}\right) \Gamma(3) D_m^3 \\ + \left(2\delta V\, D_i - 2cD_i^{1+d}\left(\frac{\rho_o}{\rho}\right)^{0.5}\right) \Gamma(2) D_m^2 + \left(\delta V\, D_i^2 - cD_i^{2+d}\left(\frac{\rho_o}{\rho}\right)^{0.5}\right) \Gamma(1) D_m^1 \end{array} \right]}$$

Appendix E: Maximum fall times and distances

Using the snow aggregate mass growth rate,

$$\frac{dM}{dt} = \frac{\pi}{4}(D_a + D_i)^2 \left|V_a - V_i + \delta V\right| E\, r_i\, \rho, \qquad \text{(equation 8)}$$

derived in chapter 2, the fall times and distances of aggregates growing to precipitable sizes are determined. In nature precipitation reaches the surface in times as fast as 15 min for rain and 30 min for snow. In order to ensure that the equations developed for the collection process of precipitation particles, the fall times and distances are considered.

Rogers and Yau (1989, p.130 and 131) outline a method for determining the fall times and distances of a raindrop growing to a specified size. This method involves integrating the mass growth rate with respect to diameter, which takes into consideration that the terminal velocity and cross-sectional area changes with size. The calculations also implement two assumptions: (i) background cloud droplets have a negligible diameter such that the cross-sectional area is only a function of the collector drop; and (ii) the fall velocity of the background cloud droplet is approximately equal zero, so the differential fall velocities between the collector and collected particles equal the collector particle's fall velocity.

Now because snow aggregates of the same shape have similar velocities regardless of size, the latter assumption can not be made when determining the fall times and distances of growing snow aggregates. Neglecting this assumption, however, leaves a complex integral so for simplicity we determine the fall time of snow aggregates using:

$$\textbf{Mass}_{\text{final}} = \textbf{Mass}_{\text{initial}} + \left(\frac{dm}{dt} \times \textbf{time}\right)$$

In doing so, however, we include the assumptions: (i) the fall velocity of an ice particle is that of its initial diameter and remains constant with time (i.e., slower than it actually is); and (ii) the assumption $\left|V_a - V_i\right| = V_a$ is not made, as with raindrops, because it gives unreasonable results due to the similarities between the fall velocities of all snow aggregates and ice crystals of the same shape. Consequently, these assumptions are representative of the 'maximum' fall times and distances. The maximum fall time is given by

$$Time_{maximum} = \frac{aD_{final}^{\ b} - aD_{initial}^{\ b}}{A_{initial}\left(\left|V_{a\ initial} - V_i\right| + \delta V\right) r_i E \rho}$$

$$Time_{maximum} = \frac{aD_{final}^{\ b} - aD_{initial}^{\ b}}{\frac{\pi}{4}(D_{a\ initial} + D_i)^2 \left(\left|cD_{a\ initial}^{\ d}\left(\frac{\rho_o}{\rho}\right)^{0.5} - cD_i^{\ d}\left(\frac{\rho_o}{\rho}\right)^{0.5}\right| + \delta V\right) r_i E \rho}$$

$$Time_{maximum} = \frac{aD_{final}^{\ b} - aD_{initial}^{\ b}}{\frac{\pi}{4}\left[\begin{array}{l}\left(c\left(\frac{\rho_o}{\rho}\right)^{0.5}\right)D_{a\ initial}^{\ 2+d} + \left(\delta V - cD_i^{\ d}\left(\frac{\rho_o}{\rho}\right)^{0.5}\right)D_{a\ initial}^{\ 2} + \\ + \left(2cD_i\left(\frac{\rho_o}{\rho}\right)^{0.5}\right)D_{a\ initial}^{\ 1+d} + \left(2\delta V D_i - 2cD_i^{\ 1+d}\left(\frac{\rho_o}{\rho}\right)^{0.5}\right)D_{a\ initial} \\ + \left(cD_i^{\ 2}\left(\frac{\rho_o}{\rho}\right)^{0.5}\right)D_{a\ initial}^{\ d} + \left(\delta V D_i^{\ 2} - cD_i^{\ 2+d}\left(\frac{\rho_o}{\rho}\right)^{0.5}\right)\end{array}\right] r_i E \rho}$$

Aggregation Zone Depth = Velocity x Time

$$\Delta z = (V_{t,a} - Updraft) \times time$$

Therefore,

$$\text{Distance}_{maximum} = \left(cD_{a\ final}^{\ d}\left(\frac{\rho_o}{\rho}\right)^{0.5} - Updraft\right) \times time_{maximum}$$

(Assumptions: r_i and updraft are constant.)

By looking at the maximum fall times and distances, we have an upper bound and if the maximum times are comparable with observations, then we can assume all fall times and distances derived are reasonable. The maximum fall times and distances required for plates and dendrites to grow from 0.005 to 0.15 cm in diameter are plotted in Figure 7.1.

Figure 7.1 shows that the fall times for plates (-8 to 0°C) and dendrites (-25 to -12°C) decrease with increasing temperature. The fastest fall time reaches 8.5 min at -12°C, with a secondary local minimum of 15.4 min at 0°C. The fastest fall times occur at the upper temperature limits of the dendritic and planar ranges, because the fall times are a function of the change in mass (ΔM) to the mass growth rate ($^{dM}/_{dt}$), and the maximum collection efficiency in the upper temperature limits equals a minimum in the

fall times. The fall times of plates and dendrites are equal from -22 to -16°C and -8 to 0°C because the ratios of the change in mass to the mass growth rate are equal. Sector plates take the longest to grow, with the minimum fall time above 50 min and a maximum fall time of 63.4 min at -10°C. The fall time at -10°C is longer than at -11°C, despite a decrease in collection efficiency. This is because snow aggregates at -11°C have a slightly greater dendrite composition than snow aggregates at -10°C, and therefore have a lighter mass which acts to decrease the fall time. These results suggest that the lighter mass of dendrites makes them more conducive to the formation of snow aggregates than plates and sector plates. Furthermore, the results in Table 2.3 indicate that the fall velocity, over all temperatures, has a greater impact on ice crystal growth than the collection efficiency. This is supported by the significant increase in fall times over the temperatures -8 to -12°C, associated with a higher ratio of mass to fall velocity and collection efficiency, compared to the relatively smaller increase in fall times at temperatures warmer than -8°C or colder than -12°C.

In Figure 7.1 the maximum fall distances are plotted for the control case and for a collection rate with an updraft of 50 cm s^{-1}. The fall distances, with and without an updraft, for plates (-8 to 0°C) and dendrites (-25 to -12°C) decrease with increasing temperatures. For the control case: (i) the shortest fall distance of 0.3 km occurs at -12°C with a secondary local minimum of 1.0 km at 0°C; and (ii) the greatest fall distance of 3.3 km occurs at -10°C. For the updraft case: (i) the shortest fall distance of 0.1 km occurs at -12°C with a secondary local minimum of 0.6 km at 0°C; and (ii) the greatest fall distance of 1.5 km moves to -9°C. The change in maximum fall distance from -10 to -9°C is because the 50 cm s^{-1} updraft has a greater effect on the sector plates at -10°C; whose fall velocity is slower than the sector plates at -9°C. Recall that the increased dendritic properties of sector plates at -10°C include a decrease in fall velocity. A reduction in fall velocity implies the snow aggregate does not cover the same distance it would without an updraft, and because the fall times remain the same, the fall distance decreases. Because sector plates and dendrites fall slower than plates, the updraft has a greater affect on their fall distances.

The fall distances of the control case ranges from 0.3 to 3.3 km while the case with an updraft ranges from 0.1 to 1.5 km. In the case without an updraft, the fall

distances are greater than 1 km for temperatures -25 to -20°C and -12 to 0°C; above 2.0 km for temperatures -11 to -6°C; and above 3.0 km for -10°C. All distances are within the 0.1 to 4.4 km reported by Magano (1960).

The values plotted in Figure 7.1 are given in Table 2.3 along with observations from Rogers (1974). The works of Rogers (1974) reported fall times ranging from 5 to 33 min at -10°C, 2 to 43 min at -13°C, and 6 to 49 min at -15°C. Note that the lower limit of the fastest fall times is observed near -12°C. By comparison, the upper limit of the fastest fall time is at -10°C and increases with decreasing temperature. The fall times of Rogers (1974) are similar to those of Khain and Sednev (1995) who found snowflakes began to form after 20 min and have a maximum melted diameter of 200 to 300 μm at the surface after 35 to 40 min.

Table 2.3 A comparison of the fall times and distances of the control case's 'maximum' results and Rogers (1974).

	Rogers (1974)		Control Case		
Temperature (°C)	**Fall Time (min)**	**Depth of aggregation zone (km)**	**Fall Time (min)**	**Depth of aggregation zone (km) No Updraft**	**Depth of aggregation zone (km) Updraft = 50cm/s**
-8 to 0°C	N/A	N/A	15.4 to 37.1 min	1.0 to 2.5 km	0.6 to 1.4 km
-11 to -9°C	At -10°C: 5 to 33min	At -10°C: 0.3 to 1.9km	51.2 to 63.4 min	2.7 to 3.3 km	0.9 to 1.5 km
-25 to -12°C	At -13°C: 2 to 43min At -15°C: 6 to 49min	At -13°C: 0.1 to 2.4km At -15°C: 0.3 to 2.8km	8.5 to 52.0 min	0.3 to 1.9 km	0.1 to 0.3 km

Comparing the values in Table 2.3, note that the fall times of Rogers (1974) at -13 and -15°C are within the fall times of the control case. The fastest fall times of Rogers (1974) and the control case both occur near -12°C. The fall times of the control case, from -11 to -9°C, are approximately double that of Rogers (1974) at -10°C, although the fall times for the control case, from -8 to 0°C, are similar. Keep in mind these fall times and distances represent an upper limit, because the values are calculated using the minimum fall speed, and the similarity to Rogers (1974) indicates that our results are reasonable.

The fall distances of Rogers (1974) and the control case both have the shortest fall distance near -12°C. Otherwise, fall distances less that 1 km only occur at temperatures colder than -12°C. In contrast, Rogers (1974) found that fall distances less than 1 km occurred at -10, -13, and -15°C.

Summary

As a result of the mass growth rate, the maximum fall times required for an ice particle to grow by aggregation from 0.005 to 0.15 cm in diameter takes less than 65 min throughout all temperatures. It is fastest for dendrites, followed by plates and sector plates. The maximum fall distances for the non-updraft case, ranges from 0.3 to 3.3 km and 0.1 to 1.5 km for the case with an updraft of 50 cm s^{-1}. The fall distances and fall times are similar to those of Rogers (1974) in that (i) the shortest fall distances are for dendrites, followed by plates and sector plates; and (ii) the distances are shortest as the temperatures near 0°C. All maximum fall times and distances are reasonable when compared to Rogers (1974), and Khain and Sednev (1995).